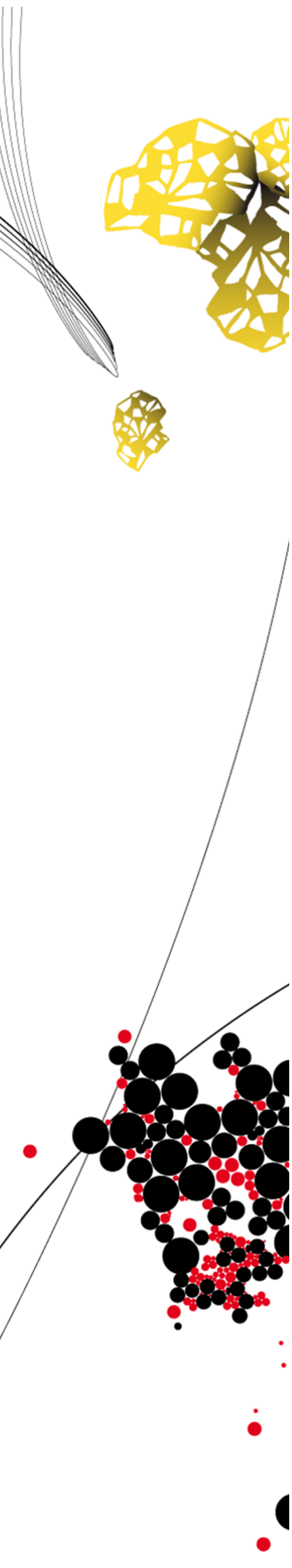

UNIVERSITY OF TWENTE.

Faculty of Electrical Engineering,
Mathematics & Computer Science

Feasibility study for a CMOS integrated Optical Receiver for FLIM

M. Duiven

MSc. Thesis
15-02-2011

Supervisors
prof. dr. ir. B. Nauta
dr. ir. A.J. Annema
dr. ir. H. Offerhaus

Report number: 067.3393
Chair of Integrated Circuit Design
Faculty of Electrical Engineering,
Mathematics and Computer Science
University of Twente
P.O. Box 217
7500 AE Enschede
The Netherlands

Abstract

A feasibility study for a CMOS integrated Optical Receiver for the application 'FLIM' is performed. FLIM stands for Fluorescence Lifetime Imaging Microscopy and is a technique that produces an image of a biological cell or tissue. Each pixel of the produced image is based on the exponential decay rate of the fluorescence of a molecule; fluorescence is the emission of light by a molecule that has absorbed light. The exponential decay rate of fluorescence is unique for each molecule.

The receiver, which performs a measurement for one pixel, should be able to process the very low power optical signal to a digital value that corresponds to a unique molecule. The aim is to produce a high resolution image for Cell imaging, for which a high resolution matrix (both spatial and in time accuracy) of receivers is required. The main challenge is to design a very low noise and low area consuming receiver.

Several methods in respectively time- and frequency-domain are analyzed and compared. Two methods are worked out in detail and are optimized at circuit and system level, leading to an estimate of a feasible resolution as function of the given optical input power density.

Contents

Chapter 1

Introduction

Optical receivers are used in many applications and in many forms. These receivers use electromagnetic light waves as information carriers. Examples of nowadays common used applications are infrared (IR) and optical fiber communication. The first is an example of wireless communication and the latter an example of communication with a wire as medium. Another distinction that can be made between different optical receivers is the modulation of the information carrier. The information can be modulated as a digital or as an analog signal. Digital modulation is mainly used in nowadays common optical communication. Only few levels have to be distinguished in that case to provide reliable communication. This relaxes the requirements of the receiver of such a system in comparison with analog modulation.

In this thesis the feasibility of a CMOS integrated optical receiver for a specific application is explored. The specific application is determined in accordance with the Optical Sciences group of Twente University. A research direction of this group is the study of the interaction of light and matter at nanoscale. A possible method to gain information about a matter at nanoscale is to measure the lifetime of the fluorescence of a matter. This is called Fluorescence Lifetime Imaging Microscopy (FLIM). This is taken as application for this thesis and is described in the next section. The required information is situated at arbitrary analog levels and received through air as medium for this application and therefore an analog wireless receiver is needed for this application.

1.1 Fluorescence Lifetime Imaging Microscopy (FLIM)

To explain what Fluorescence Lifetime Imaging Microscopy exactly implies, firstly it is explained in broad lines what Fluorescence is.

Fluorescence is a molecular luminescence process in which molecules spontaneously emit a photon as they relax from an excited electronic state to their ground state following absorbtion of energy [1]. The characteristic electronic states and relaxation process involved in fluorescence emission are illustrated in figure 1.1.

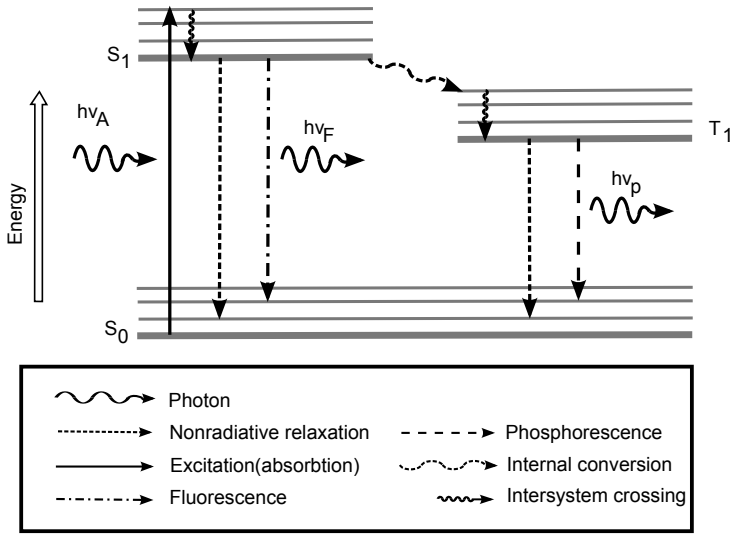

Figure 1.1: A Jablonski diagram representing the energy levels of a fluorescent molecule and several important transitions[1]

A molecule contains fluorophores. These are components that cause a molecule to be fluorescent. These components absorb photon energy of a specific wavelength and re-emit energy at different wavelength, called fluorescence. The fluorescence emitted will decay with time. The fluorescence lifetime is the signature of a fluorescent material; it's the exponential decay in emission after the excitation of a fluorescent material. In other words, the lifetime is the average time that fluorescent molecules spend in the excited state.

The local concentration of fluorophores, the local excitation light intensity, the optical path of the microscope and the local fluorescence detection efficiency are not of influence on the lifetime measurements because the fluorescence lifetime does not change upon intensity variations. The fluorescence decay develops according to (1.1)[1].

$$f(t) = F_0 \cdot e^{-\frac{t}{\tau}} \tag{1.1}$$

where τ is the fluorescence lifetime and F_0 is the initial fluorescence at t=0. It is shown in the above equation that the fluorescence emission is dependent on the variables F_0 and τ and therefore the detection of these variables is sufficient to identify the measured matter. In specific cases, fluorophores change their quantum yield upon the interaction with other fluorescent molecules. This influences the fluorescence lifetime of the analyzed matter. FLIM can measure this lifetime dynamics and can therefore measure indirectly biomolecular concentrations and interactions that are closely related to the fluorescence lifetime of the fluorophores [1].

FLIM can be used for many applications. Several are listed:
The measurement of

- quantitative determination of ion concentrations
- pH
- oxygen content
- protein-protein interactions
- cell motility
- cancer diagnosis

The measurement of the fluorescence lifetime can be performed on several ways. In [1] different methods are described. The methods can be roughly divided into time-domain FLIM and frequency domain FLIM.

With frequency-domain FLIM described by [1], the intensity of the excitation light is continuously modulated. The fluorescence emission will display a phase shift and a decrease in modulation due to the fluorescence decay. These modulations and consequently the fluorescence lifetime can be extracted in the frequency domain. The modulated fluorescence signal is usually measured using a photo multiplier tube and a CCD camera. This method is described in detail in appendix A.

With time-domain FLIM the fluorescence lifetime is measured after exciting the matter with a short light pulse according to [1]. The resulting decay curve is described by (1.1). By recording the arrival time of the emitted photons, a representation of the decay curve is obtained. The measurement is usually performed using time correlated single photon counting (TCSPC).

1.2 Design of an optical receiver

The Optical Sciences group of Twente University use time-domain FLIM to analyze matter and this method is therefore also analyzed and implemented for this research. The matter to be analyzed is excited with a pulse train at a frequency of 80MHz. This frequency is chosen for practical reasons (and is determined by the Optical Sciences group) and is assumed fixed for this assignment.

A disadvantage of the current measurement systems is that the measurement time is relatively long and the measurement equipment is big (in comparison with an integrated solution). The aim of this project is to investigate the feasibility of the use of an optical integrated CMOS radio for this application.

To measure the properties of matter and reflect this in a picture with a high resolution, a receiver that scans the matter or a matrix of receivers is needed. The scanning method is very time consuming and complex and therefore a matrix of receivers is investigated. The design of the whole matrix of receivers falls out of the scope of this thesis and therefore one receiver that corresponds with one pixel and can easily be implemented in a matrix is investigated and designed. The receiver should be designed such that the design can be simply

copied and combined to form a matrix in one IC. Because the resolution of the receiver matrix should be high, the hardware overhead and the power consumption of one receiver should be low.

Several requirements and properties for the optical receiver can be deduced from the application discussed above.

- The received information is modulated as an (analog) exponential decay at a modulation frequency of 80MHz.
- The information of the received signal is carried in the τ and constant F_0 (see (1.1)) of the exponential decay signal.
- The receiver should be integrated in a CMOS process.
- The resolution of the τ extraction should be below 100ps.
- The hardware overhead and power consumption should be low.
- τ-range: 1-10ns

With conventional measuring devices for FLIM based cell imaging, a cell of 100μm x 100μm is imaged with 100x100 (10k) pixels. The optical power that is received at each pixel is 5nW and the duration of the measurement is limited to 1ms. The total power per sample therefore equals 50μW. The aim of this project is to investigate the feasibility of producing an image with comparable properties as the conventional measurement devises with an integrated receiver.

1.3 Acknowledgements

First of all I would like to thank Anne-Johan Annema for providing me with this assignment and supervising this master thesis project. The meetings with him provided me with much interesting and useful information and feedback. Also I would like to thank Herman Offerhaus for providing the very interesting application for this master thesis assignment and for attending my graduation committee. Furthermore I would like to thank the good people from the ICD group, both staff and students. Especially I would like to thank Bram Nauta, Gerard Wienk, David Borggreve, Frederik van den Ende, Arjan van Heusden and Rien Oortgiessen, and thank them for their feedback and advice. Finally I would like to thank Anita Kleene for her patience, support and for providing me with positive energy during the past few months.

1.4 Thesis outline

First the problem description and a quantitative analysis of the received signal will be addressed in Chapter 2 to provide the requirements for the system design methods that are mathematically analyzed in Chapter 3. In Chapter 4 these methods are compared at a circuit implementation level point of view and the two most suitable methods are designed and analyzed at circuit level in Chapter 5. Chapter 6 provides the optimization of one of this circuits and finally the conclusions are presented in Chapter 7.

Chapter 2

Problem description and quantitative analysis

In this chapter first the main problems for this feasibility study are described. Subsequently the received signal is quantitative analyzed in the time- and frequency domain such that methods that are appropriate to solve the problem can be investigated. This last step is performed in chapter 3.

2.1 Problem description

Just as many roads lead to Rome, there are many ways to perform the reception of analog signals and conversion to the digital domain. It is an art to find the most optimal way (and in case of the road to Rome the most optimal road). To find the most optimal solution, many (good) choices have to be made. However these choices are affected by multiple factors. Some (important) factors, properties and requirements, are listed below:

- IC technology
- Time domain behavior of the received signals
- Frequency domain spectrum of the received signals
- Power range of the received signals
- Received quantity
- Accuracy requirements
- Power dissipation requirements
- Area requirements

The first five items are more or less fixed for this application. The properties and behavior of the received signals are defined by measurement set-ups currently used by the Optical Science group. Only the design of the receiver is treated in this thesis and therefore these factors are fixed. The used IC technology is application dependent. Important factors are the availability

of IC technologies, which technology is most suitable to combine with digital electronics and which technology is most suitable for the measurement of the received quantity. The NXP 'ABCD9' CMOS process is used because this process achieves very good photon to electron conversion efficiency and good analog and digital performances.

The last three items in the list are not fixed and are treated as variables for this feasibility study and system/circuit design. Because this thesis presents a feasibility study, it is investigated which figures are achievable. It is always a trade off for which variable the design is optimized. The accuracy of the measurement is among other things determined by the resolution of the receiver matrix. It is investigated which resolution is achievable and this has direct effect on the power dissipation and area requirements. To achieve a resolution as high as possible, the power and area consumption should be as low as possible. Further investigation should point out both the exact figures of these constraints and the hardest constraint.

2.2 Quantitative analysis

The choices that have to be made for a proper receiver design are heavily influenced by the properties of the received signal. Therefore the time- and frequency-domain specifications of the received signal are determined in the next subsections.

Time-domain Specifications

The time domain behavior of the fluorescence decay of analyzed matter is described by (1.1) and shown in figure 3.1. As described in the previous chapter, specific values of the lifetime (τ), or specific decay rates, correspond to specific matter. Because the matter is excited with a light pulse modulated at 80MHz, the received signal is a periodic exponential signal. The algebraical description of this signal is derived in appendix G, yielding expression 2.1 for one period.

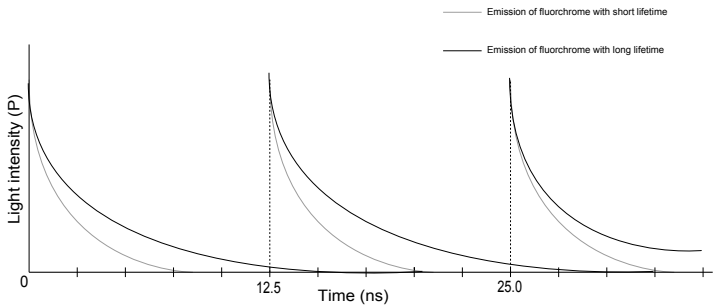

Figure 2.1: Graphical representation of time-domain behavior of fluorescence emission at a repetition frequency of 80MHz

$$f_p(t) = F_0 \cdot e^{-t/\tau} \cdot \frac{1}{1 - e^{-T/\tau}} \tag{2.1}$$

Frequency-domain Specifications

The optical input signal can also be described in the frequency-domain, which is required for retrieving τ using frequency domain algorithms. This algebraical analysis is also performed in G and yields the expression shown in (2.2) and figure 2.2.

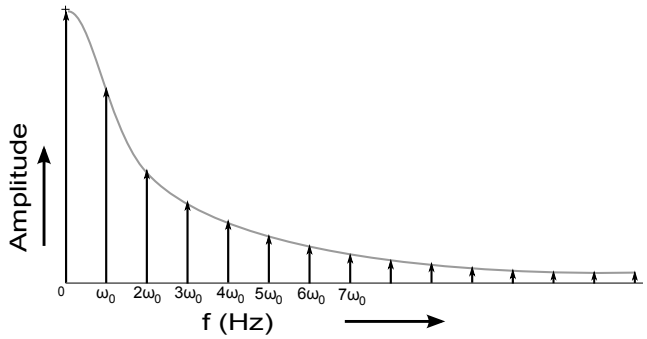

Figure 2.2: Frequency behavior of (1.1), described by (2.2)

$$H(\omega) = \frac{F_0}{\frac{1}{\tau} + i\omega} \cdot \frac{1}{T} \sum_{k=-\infty}^{\infty} \delta(f - \frac{k}{T}) \tag{2.2}$$

Numerical simulation are performed to verify the correctness of the derivation by comparing this result with a real time measurement. The results with $\tau = 2ns$ and $F_0 = 1$, are given in figure 2.3. Figure 2.4 shows results from

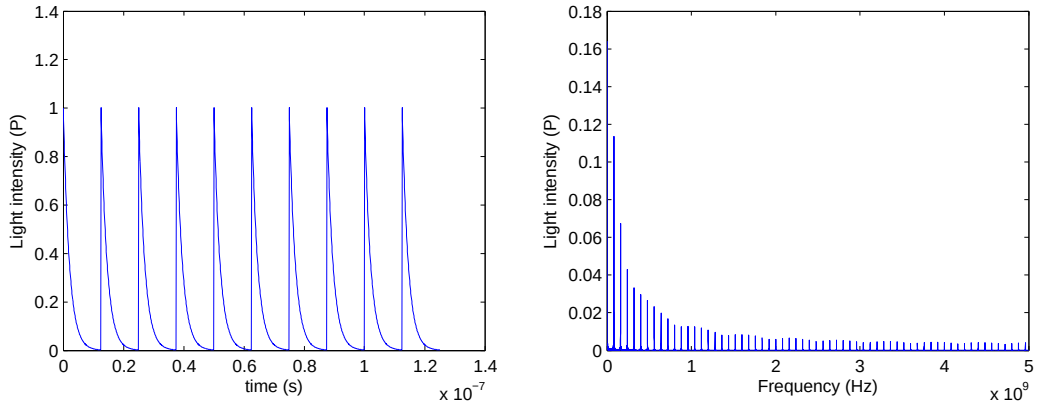

(a) Time-Domain (b) Frequency-Domain

Figure 2.3: Graphical representation of the periodic signal in the time- and frequency-domain obtained with MATLAB.

a real time measurement [2], which nicely comply to the calculated results of figure 2.3.

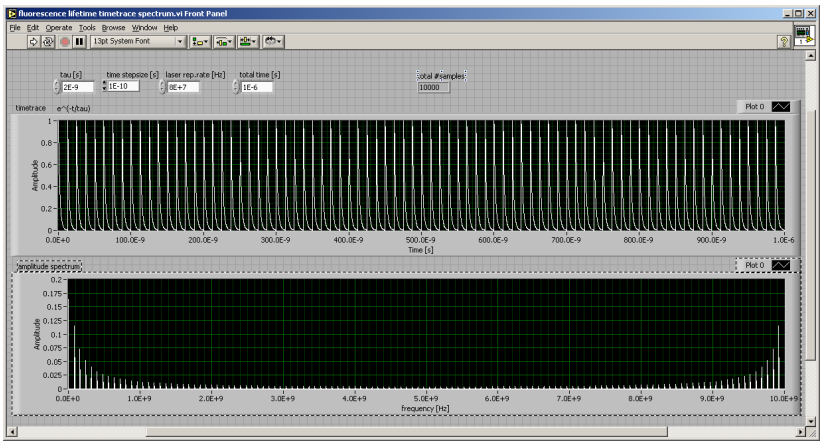

Figure 2.4: real-time measurement

Chapter 3

System design methods

3.1 Description of System design methods

The aim of one optical receiver is to produce a pixel of an image based on the exponential decay rate of the fluorescence from a fluorescent molecule. The exponential decay rate is reflected by the variable τ and the value is unique for each molecule. Extracting τ from the received signal is sufficient to obtain the wanted properties of the analyzed matter[3]. In this section the most suitable methods, from an electronics implementation point-of-view, to extract τ from the measured signal are determined.

It is investigated if and how τ can be extracted with several methods in this section; in section 3.2 the influence of measurements errors (timing errors and magnitude errors) on the accuracy of the extraction of τ is investigated, and the methods are compared.

The received signal can be described in the time- and frequency-domain and therefore the methods can be classified in the concerned domain. The time-domain methods that are analyzed are:

- Measurement of two time-samples
- Two area measurements
- Two average area measurements
- Area measurement combined with a time-sample

The frequency-domain methods that are analyzed are:

- Measurement of two frequency-samples
- I and Q frequency sample measurement

A method that combines both domains is also analyzed; an time-domain area measurement is combined with a frequency-sample measurement.

The four time-domain methods to extract τ from the received signal listed above are mathematically elaborated in appendix D.1.1, the frequency-domain methods in appendix D.1.2 and the method that combines both domains in D.1.3.

The mathematical analysis shows that all elaborated methods are mathematically solvable except the method that combines an area measurement with a time-sample measurement and the method that combines both domains. This means that the value of τ can be algebraical obtained if real time measurements for the concerned method are performed. The analysis also shows that performing two measurements is sufficient to determine the value of τ for all solvable methods. The expressions needed to calculate τ (derived in appendix D.1) are listed in table 3.1 and the time domain methods are visualized in figures 3.1. The frequency behavior the received signal is shown in figure 3.2. The analysis performed in D.2 describes that measuring two arbitrary independent frequency components given in figure 3.2a is sufficient to extract τ for the 'frequency sample' method. It is also described that measuring the imaginary and real part of an arbitrary independent frequency component for the 'I and Q frequency sample' method is sufficient to extract the value of τ. The behavior of the real and imaginary part of the received signal in the frequency domain is given in respectively figure 3.2b and 3.2c.

Method:	Expression
two time-samples	$\tau = \frac{t_1 - t_2}{ln\left(\frac{f(t_2)}{f(t_1)}\right)}$
Two area's	$\tau = -\frac{C}{ln\left(\frac{A(t_3,t_4)}{A(t_1,t_2)} - C_3\right)}$
Two average area's	$\tau = -\frac{C}{ln\left(\frac{AA(t_3,t_4)}{AA(t_1,t_2)} \cdot \frac{t_2 - t_1}{t_4 - t_3} - C_3\right)}$
Frequency-samples	$\tau = \sqrt{\frac{\left(\frac{\lvert K(\omega_2)\rvert}{\lvert K(\omega_1)\rvert}\right)^2 - 1}{\omega_1^2 - \left(\frac{\lvert K(\omega_2)\rvert}{\lvert K(\omega_1)\rvert}\right)^2 \cdot \omega_2^2}}$
I and Q frequency	$\tau = \frac{b_n}{n\omega_0 a_n}$

Table 3.1: Expression to extract τ for the elaborated methods

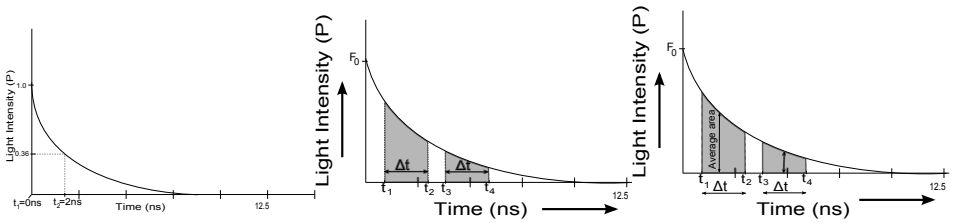

(a) Samples (b) Area (c) Average Area

Figure 3.1: Time domain measurements

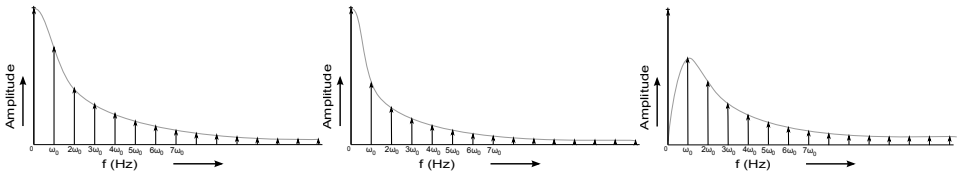

(a) Complex signal (b) Real part (c) Imaginary part

Figure 3.2: frequency domain behavior

3.2 Accuracy and comparison of system design methods

The influence of measurement errors, which are grouped in timing and magnitude errors, on the accuracy of the extraction of τ is investigated in this chapter. Also the most optimal values for some variables in the receiver (sample times, integration limits and modulation frequency) are derived to acquire maximal independency for measurement errors. From the analysis of the impact of these measurement errors, a first selection of the algorithms listed in section 3.1 is done to obtain the most robust algorithms.

In this section the inaccuracy of τ is represented as an absolute error (ϵ_τ) and is described as function of the measurement errors. A requirement of the receiver design is that the lifetime of each matter is measured with a resolution of 100ps. To obtain this resolution the τ measurement error may not exceed 49ps. Because the maximal permitted τ-error is fixed, the maximal allowed measurement errors can be estimated.

The relation between the measurement errors and the resulting τ-error is described for all methods that are treated in 3.1. Most of the described methods suffer from multiple measurement errors, mainly timing and magnitude errors. The measurement errors are mutual dependent and therefore it is very difficult to obtain the most optimal variable values that allow maximum values for both measurement errors. However the timing errors are mainly caused by one circuit block: the phase-locked-loop (PLL). A literature study (see appendix D.3) shows a typical 5ps timing error. This value is from now on used as constant. Because the timing error is now described by a constant and the magnitude error as a variable, the τ extraction method with the best feasibility can be selected by deriving and comparing only the maximal allowed magnitude errors for each method. In this chapter, the magnitude errors in time and frequency domain are specified in a normalized way, in signal-to-noise ratio (SNR).

Magnitude errors are caused by different mechanisms. These mechanisms can be grouped into two main categories: deterministic and random errors. The deterministic errors are among other things caused by gain errors and offset errors and can be measured with a 'zero' measurement and compensated during real time measurement. The random errors mainly caused by (white) noise. Noise has a Gaussian distribution and therefore about 99.7% of all noise errors are within three times the standard deviation (3σ) away from the mean value.

Therefore the magnitude error introduced by noise can be described by a variable that accounts for a percentage of the total error and can be positive or negative. If the allowed magnitude errors are obtained, the maximal allowed noise can be calculated.

The expressions for the maximal allowed magnitude errors and minimal achievable signal-to-noise ratio are derived in appendix D.2 and the optimal variable values and maximal allowed magnitude errors are obtained in appendix D.3. Substituting the optimal variable values, the obtained timing error (5ps) and the maximal allowed τ-error (49ps) in the expressions obtained in appendix D.2 and D.3 give the maximal allowed magnitude error and minimal required SNR presented in table 3.2. The figures in this table show that the Area- and I/Q measurement methods do not meet the formulated specifications and are therefore no option for further investigation. The combination of the area method with the frequency sample method yields equal performance as the frequency sample method. This is because the area of the whole period should be measured and this corresponds with the DC component in the frequency domain. In essence both methods are equal and therefore only the frequency sample method is elaborated further on. The practical implementation of the

	ε_{mag}	SNR	SNR_{dB}
Time sampling	0.92μ	$1.08 \cdot 10^3$	60.7dB
Area Meas.	-	-	-
Average Area	0.81μ	$1.2 \cdot 10^3$	61.8dB
Freq. sampling	0.32μ	$3.1 \cdot 10^3$	69.9dB
I/Q meas.	-	-	-
Area + Freq.	0.32μ	$3.1 \cdot 10^3$	69.9dB

Table 3.2: List with maximal permitted error and minimal achievable SNR to obtain maximal a 49ps τ-measurement error

methods in the different domains yield different advantages and disadvantages and therefore a decision which method is best suited for full integration in CMOS technology is not made at this moment. In chapter 4 the methods are compared at in implementation level point of view and one method is selected.

Chapter 4

System design choice

In the previous section all possible methods are described and compared. Table 3.2 shows the allowed accuracy, reflected as allowed magnitude error and SNR, of each method. The most optimal method can extracted from the accuracy reflected in this table if it can be assumed that the measurement errors are equal for each method. This is however not the case at a practical implementation level. Therefore the influence of practical properties on the measurement accuracy also have to be taken into account. This is performed in this chapter by elaborating the methods into a system design and describe and compare the practical properties of each system. Table 3.2 however does show that some methods are not feasible and these methods are not further investigated.

The systems should meet multiple requirements to be suitable for this application; they should be feasible to form a high resolution matrix, the resolution of the τ extraction should be high enough (100ps) and the measurement should be performed within a limited time (approximately 1ms). To meet these requirements the area needed for the receiver and the amount of random noise that will be present at the output should be reduced to a minimum and the settling time of the system should also be limited. Therefore the feasibility of the described systems is compared taking these requirements into account.

Deterministic errors, like offsets are in many applications also a problem. For this application however a calibration can be performed to measure the deterministic errors and save the values very accurate in the digital domain. During real time measurement these errors can be subtracted from the measured quantities. Therefore these errors are not taken into account during this feasibility consideration.

Different system designs can be thought of for the implementation of the feasible methods. Several possible systems are discussed. The properties of each system are listed and subsequently the systems are compared.

System1: Measurement of two time samples

In figure 4.1 the system of the *Two time sample method* is shown. The receiver contains a diode and a transimpedance amplifier (TIA) to convert the received

optical power to a voltage. Two (almost) identical branches subsequently perform the two sampling measurements. A sample-and-hold circuit (S&H) performs the sampling at a specified moment and is steered by a clock-signal with the same frequency for each branch which is equal to the fundamental frequency of the received signal (80MHz). The clocks are shifted with a certain delay compared to each other.

An analog-to-digital converter (ADC) and a digital signal processing (DSP) block respectively convert the measured samples to the digital domain and perform some digital signal processing at last.

As already stated, measuring many periods decreases the influence of the random errors. Therefore each measured sample should be converted to the digital domain and subsequently the mean value of as many samples as possible has to be determined in the DSP. Taking the average of many samples is in essence a low-pass filter operation. This can be performed for all systems in the digital domain.

Any sampling circuit consist of at least of a switch and a capacitor. The switch has a finite on-resistance which generates thermal noise. The noise is filtered by the low-pass circuit formed by the on-resistance and the sampling capacitance. Integrating the noise spectral density weighted by the low-pass transfer yields the mean square noise voltage on the capacitor. This is equal to the well known kT/C noise. The sampling operation aliases all the noise energy, so also the noise generated in previous circuits, into the Nyquist band ($F_S/2$) [4]. A disadvantage of this method is that the settling-time and thus the capacitance of the (S&H) circuit should be small, consequently much noise energy will be present in the Nyquist band. Properties of this system:

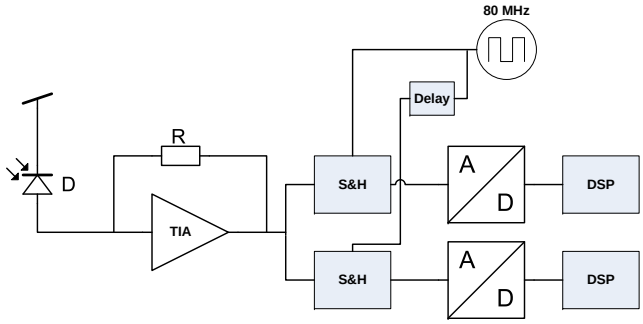

Figure 4.1: System of the *Two time sample method*

- Two ADC's at 80MHZ or sharing a ADC at higher frequency
- averaging in DSP needed
- Minimal SNR: 67dB
- Deterministic timing errors that are common for both samples do not influence the measurement
- Noise aliasing
- High TIA bandwidth ($\geq$1GHz)

System2: Two average area measurements

The system of the *Two average area method* is shown in figure 4.2. The system measures the average area of an defined part of the exponential function. The diode and TIA are followed by two identical branches with a switched low-pass RC-filter. The RC low-pass filter measures the average area of the defined part of the period. The received signal is in essence mixed with a periodic pulse signal while performing the sampling operation. The spectrum of a periodic pulse signal incorporates frequency components at multiples of its fundamental frequency and the magnitude is shaped by a sinc signal. This causes that the frequency components of the received signal are mixed to DC by the corresponding component of the periodic pulse. The magnitude of both the received and periodic pulse signal decrease with increasing frequency consequently the most significant information is present at the first components. The measurement error however should be small and therefore the information present in the higher frequency components is also of importance for an accurate measurement. Because of this, the bandwidth requirement of the TIA is high. After the sampling operation, the required information is only present at DC. Components are however still present at all other integer multiples of the fundamental frequency and therefore the low-pass filter should attenuate these unwanted components heavily. Properties of this system:

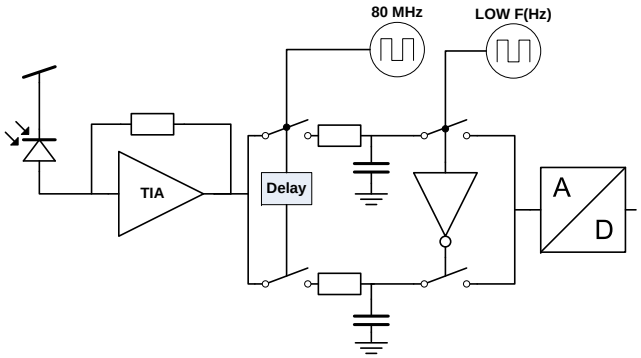

Figure 4.2: System of the *Two average area method*

- One ADC at very low frequency (max several kHz) that can be shared for all receivers
- Almost no digital filtering needed if bandwidth of RC-filter is very low
- Minimal SNR: 63dB
- Deterministic timing errors that are common for both samples do not influence the measurement
- High area consuming R and C needed for low-pass filtering
- Long settling time if large R and C
- 1/f noise of TIA at DC

System3: Measurement of two frequency samples

The system of the *Two frequency samples* method is shown in 4.3. In chapter 3 it is determined that the measurement of the magnitude of the first two independent frequency components, which are situated at respectively DC and ω_0, yield best mathematical accuracy for this method. A disadvantage of measuring the DC component is that the 1/f noise of all active devices will degrade the DC measurement. It is shown in table D.2 that the mathematical accuracy however degrades with a factor 50 if another component instead of the DC component is measured.

The system performs the measurement of both components in two branches. The upper branch measures the component situated at DC and the lower branch measures the component situated at ω_0. The upper branch uses a low-pass filter to attenuate the components following the DC component. Subsequently the DC-level is converted to a digital signal and processed in the DSP. The lower branch mixes the component situated at ω_0 to DC or low-IF. A low-pass filter subsequently attenuates the other components, which are situated at all integer multiples of ω_0, leaving only the wanted component situated at DC. The component is subsequently converted to the digital domain and processed in the DSP.

A disadvantage of this system is that the wanted component situated at ω_0 should be mixed to DC with a pure sinusoid. In common receivers square-waves are used as local oscillator signal because a highly linear switching mixer can than be used. A square-wave however contains harmonics at all odd integer multiples of the fundamental frequency. These harmonics will consequently mix all odd (unwanted) harmonics of the received signal to DC. Therefore the wanted component should be mixed with a pure sinusoid, which is very hard to produce, with a highly non-linear mixer. In [5] it is explained that a non-linear circuit causes intermodulation between different frequency components. The received signal contains many frequency components and consequently many (unwanted) distortion products will be generated. To solve this problem a band-pass filter can be used. This however requires much area overhead and will introduce extra noise.

The received signal is complex and therefore to mix both the real and imaginary part of the signal, the signal should be mixed with a sin (for the complex part) and a cosine (for the real part) to DC. This can be performed in succession are with two parallel mixers.

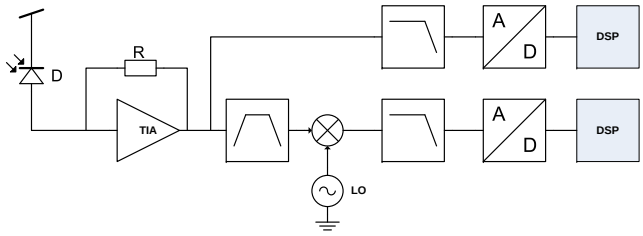

Figure 4.3: System of the *Two Frequency Sample method*

Properties of this system:

- One ADC at low frequency needed that can be shared for all receivers
- non-linearity intermodulation products or area consuming band-pass filter
- Two different gain paths
- Two low-pass filters needed to filter higher order components (≥80MHz)
- Minimal SNR: 66dB
- Smaller bandwidth TIA (≥160MHz)
- Mixing of real and complex part

System4: Measurement of two frequency samples

Figure 4.4 shows a different system for the implementation of the *Two frequency samples method*. The system performs the measurement mainly in the digital domain in contrast with the previous system. Therefore the system only filters the components other than the first and second and converts the two components to the digital domain. The DC component can be measured by low-pass filtering and the ω_0 component can be digitally mixed to DC. Properties of this

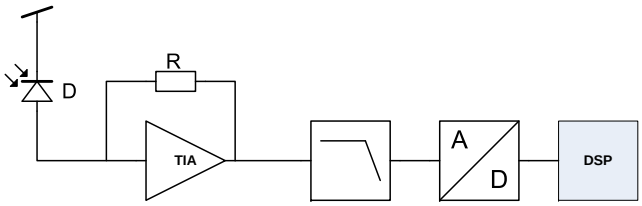

Figure 4.4: System of the *Two Frequency Sample method*

system:

- One high resolution ADC needed at high frequency (>160MHz) that can not be shared
- Very much digital signal processing needed because filtering and mixing has to be performed in the digital domain.
- Minimal SNR: 66dB
- Smaller bandwidth TIA (≥160MHz)

Comparison of the systems

At the start of this chapter it is described that the feasibility of the systems are compared taking three requirement into account next to the mathematical performance obtained in chapter 3. The three requirements are: minimal area, minimal random noise and limited measurement time (1ms).

All systems perform comparably with respect to the minimal area requirement. All systems need relative bulky filters that attenuates all components other than DC. System 4 requires a high performance ADC which can not be

shared for each receiver of the matrix and requires very much digital hardware overhead. Therefore this system is not convenient for this application and will not be taken in consideration further on.

All other systems transform the needed signals to a DC value. Therefore the influence of random noise can be minimized by low-pass filtering. This can be performed in the digital and analog domain. In the analog domain bulky capacitors are needed and in the digital domain computer processing power is needed. Processing power is available and therefore the filtering is performed in the digital domain. All systems can minimize the noise bandwidth therefore to the same extend. The systems therefore have to be compared with respect to its noise power density.

System 1 performs worst at the noise requirement. This is because all noise generated in the first circuits (TIA and $S\&H$) is folded back (due to aliasing) to the Nyquist band. Therefore this system is also not convenient for this application. System 2 suffers for both measurements from 1/f noise generated in the TIA, System 3 however suffers only from this noise for the DC component measurement. The measurement performed in the other branch however also suffers from noise and non-linearity intermodulation products generated in the mixer circuit. It is hard to predict which circuit performs best because no hard figures are available at the moment. Therefore both systems are worked out in more detail at circuit level in chapter 5.

Chapter 5

Circuit design

In this chapter the two systems obtained in chapter 4 are worked out in detail at circuit level. Taking the mathematically analysis performed in appendix D into account, optimal circuit values are obtained. Also the influence of practical limitations like limited bandwidth, non-linearity distortion and noise contribution are taken into account in the circuit design. Finally the influence of these limitations on the τ extraction accuracy is described and the feasible optical resolution is estimated.

5.1 Average area method

The system of the *Two average area method* is shown in figure 5.1. In this section first the circuit design of the 'average area method' is described detail in section 5.1.1 and subsequently the performance of the circuit is evaluated in section 5.1.2.

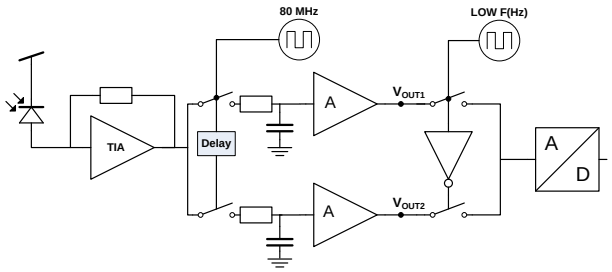

Figure 5.1: System of the *Two average area method*

5.1.1 Circuit Design

The system can be divided into multiple independent circuits:

- Photo Diode

- TransImpedance Amplifier (TIA)
- RC sampling filter
- Amplifier
- Analog-to-Digital Converter
- Digital Signal Processor

All listed circuits are described, optimized if necessary, and the influence of the practical limitations are described below. The circuits are designed and optimized with the specifications and requirements obtained in all previous chapters taken as constants. The relevant specifications and requirements are:

- The repetition frequency of the received signal is 80MHz.
- The τ extraction error should be below 50ps.
- τ-range: 1-10ns
- The received optical power per sample is 50μW
- Constant timing error of 5ps

Photo diode

The integrated photodiode converts the optical power into an electrical current; the relation for this conversion is (neglecting optical quantum noise)[6]:

$$I_{pd} = \eta_{ext} q \frac{P_o \lambda}{h\, c} \tag{5.1}$$

where h is Planck's constant, c the speed of light, λ the wavelength of the received light, q the elementary charge and η_{ext} is the external quantum efficiency which is approximately 0.4 for a photo diode integrated in the CMOS ABCD9 process. The received wavelength is dependent of the analyzed molecule and the spectral properties and therefore the optimal excitation and emission wavelength is unique for each molecule. Due to internal conversion in the excited state following excitation, the energy of the excited state is lowered and emission of longer wavelength photons takes place with respect to the excitation wavelength. These values are in the range of visible light (400-700 nm)[1].

Substituting the values in (5.1) yields an optical power to current transfer in the range of 0.12-0.22 A/W. For the worst case situation 0.12A/W is from now on taken as transfer.

Shot noise is introduced due to the conversion process; the relation of the noise density is (neglecting optical quantum noise):

$$\overline{I_{n.pd}^2} = 2q\, I_{pd} \tag{5.2}$$

TIA

A transimpedamce amplifier (TIA) converts the input current to an output voltage by its transimpedance gain, R_{TIA}:

$$V_{OUT} = I_{IN} \cdot R_{TIA}$$

Ideally this relation is linear, frequency independent and independent of its input and output load. This is however never the case in practical implementations. The performance is mainly limited by the next properties:

- Limited bandwidth
- Non-linear I-to-V transfer
- Noise contribution of the electric devices

According to the FRIIS noise equation [5] the first stages of the receiver should have maximal gain and minimal noise contribution to achieve an optimal noise performance, therefore the transimpedance should be maximal. The influence of the non-linear I-to-V transfer is small because the input amplitude is very small (see section 5.1.2). The noise contribution of the TIA is taken in consideration during the TIA design. The influence of the bandwidth limitation on the achievable transimpedance and the total accuracy is investigated below.

Limited bandwidth of the TIA:

The bandwidth of electronic devices is limited through (parasitic) capacitances and impedances. It is assumed that the photo-diode contains a parasitic capacitance of 200fF. Along with the diode capacitance, the input capacitance of the TIA and the input impedance of the TIA the input pole is formed. It is assumed that this input pole is dominant if a single stage TIA is used, and therefore the transfer of the diode and TIA is approximated by a first-order response. To estimate the influence of a limited bandwidth on the input to output transfer of the TIA the convolution of the input signal with a first order filter is obtained with a numerical analysis. The differences between the ideal input signal and the band limited output signal are reflected in figure 5.2 for different bandwidths.

The figures show that the output of the TIA more or less settles after a period which is dependent of the bandwidth of the TIA. It can be concluded from the figures that the starting time of the first integration in a period (t_1) should be sufficient to not introduce a large error. Therefore a numerical analysis is performed to estimate the influence of this error on the τ accuracy for two different t_1 values. The results, with the introduced τ-error as function of the bandwidth, for t_1=1ns and t_1=1.5ns are reflected in respectively table 5.1 and table 5.2.

In table 5.3 the minimal needed SNR to meet the required resolution is reflected as function of variable t_1. The figures in the table show that the accuracy decreases with increasing t_1 and therefore this value should be as low as possible.

The analysis reflected in table 5.1 and 5.2 show that a smaller bandwidth introduces a significant τ error and requires a higher value for t_1, but the figures

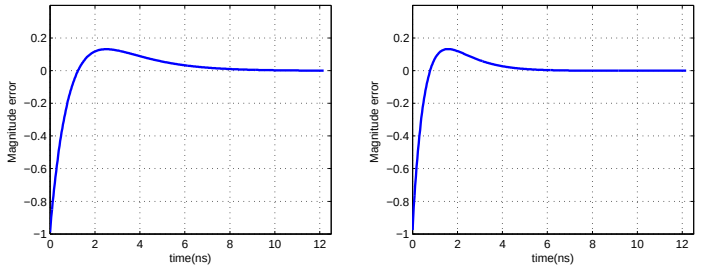

(a) BW=0.2GHz

(b) BW=0.5GHz

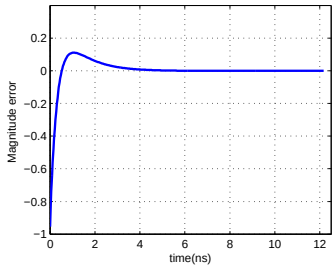

(c) BW=1GHz

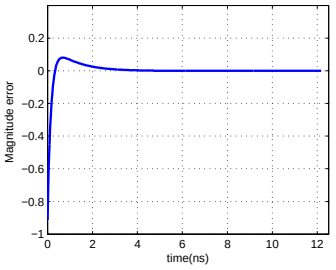

(d) BW=2GHz

Figure 5.2: Settling error introduced due to limited TIA bandwidth for different bandwidths

BW(GHz)	τ-error (ps)
0.5	5000
1	450
1.5	65
2	11

Table 5.1: t_1=1ns

BW(GHz)	τ-error (ps)
0.5	2000
1	114
1.5	8
2	1

Table 5.2: t_1=1.5ns

in table 5.1 show that a higher value for t_1 decreases the allowed magnitude error significantly. It can be concluded that a high bandwidth is required.

Common Source versus Common Gate TIA:

Two high bandwidth topologie TIA's are commonly used; the Common Source and Common Gate. A standard Common Source and Common Gate TIA are shown in figure 5.3 and the most important expressions are given in table 5.4

It is assumed that the photo diode capacitance is dominant at the input of the TIA and that C_{in} is equal for both circuits. The listed expressions show that both designs obtain approximately equal bandwidth performance (if $R_F \approx R_{D_{CG}}$, $R_{D_{CS}} \approx r_o$ and $g_{m1} \approx g_{m2}$) and transimpedance (if $R_F = R_{D_{CG}}$) , but differ at noise performance. The noise contribution of respectively R_F and $R_{D_{CG}}$ are equal, but the contribution of NMOS m1 and $R_{D_{CS}}$ is attenuated with a factor $g_{m1}^2 R_F^2$ for the common source TIA. Assuming that $R_f >> \frac{1}{g_{m1}}$,

t1	SNR
0	827
0.1	848
0.5	940
1	1086
1.5	1282
2	1562
3	2636

Table 5.3: Minimal needed SNR for different start integration time t_1

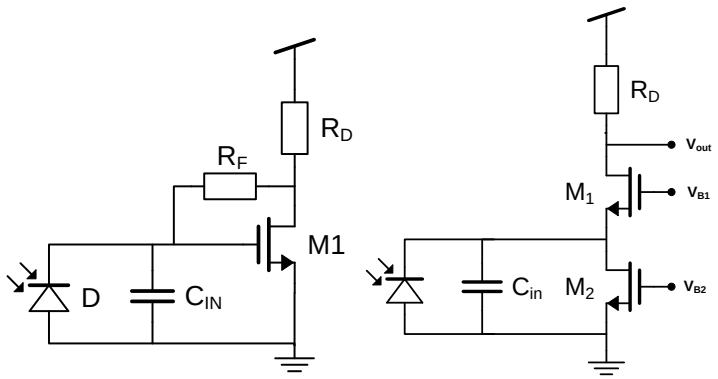

(a) Common Source TIA (b) Common Gate TIA

Figure 5.3: Common Source and Common Gate TIA

the noise contribution of the common source TIA is smaller than the noise contribution of the common gate TIA. Therefore the common source stage is used for this application.

TIA component optimization:

The transimpedance should be as high as possible (according to the FRISS noise equation [5]) as long as the bandwidth of the TIA is sufficient high to not contribute a significant τ error. In table 5.2 it is shown that a TIA bandwidth

	Common Source	Common Gate
R_{TIA}	$-\frac{g_{m1}R_f-1}{g_{m1}R_D+1}R_D \approx R_F$	R_D
BW	$\frac{1+g_mR_D}{2\pi(R_F+R_D)\,C_{in}}$	$\frac{1+g_mr_o}{2\pi(r_o+R_D)C_{in}}$
$\overline{I^2_{n,in}}$	$\frac{\overline{I^2_{n,m2}}+\overline{I^2_{n,R_D}}}{g_m{}^2R_F^2}+\overline{I^2_{n,R_F}}$	$\overline{I^2_{n,m2}}+\overline{I^2_{n,R_D}}$

Table 5.4: Relevant small signal expressions for respectively the Common Source and Common Gate TIA

of 2GHz is sufficient to not contribute a significant τ error for the specifications listed in chapter 1.2. Therefore the bandwidth of 2GHz is set as main requirement.

Furthermore the optimal values with respect to noise performance and transimpedance gain are obtained. As stated before, the transimpedance should be as high as possible to decrease the influence of the noise contribution of the next circuits. However also the noise contribution of the first stage is of importance because this is amplified by all following gain stages.

At first an optimal value for g_{m1} is obtained. According to the expressions in table 5.4 the value of g_{m1} should be maximal to acquire maximal bandwidth and transimpedance. The NMOS noise contribution is described by (5.3) and also states that a maximal g_{m1} yields minimal noise.

$$\begin{aligned} \overline{I^2_{n,NMOS}} &= \frac{4kT\, g_{m1} + \frac{K}{C_{ox} W L f} g^2_{m1}}{g^2_{m1} R_f} \\ &= \frac{4kT}{g_{m1} R_f} + \frac{K}{C_{ox} W L f R_f} \end{aligned} \tag{5.3}$$

A large g_m device however also yields a large parasitic capacitances and therefore a decrease in bandwidth. An as high as possible g_m value is taken without exceeding a parasitic input capacitance (C_{gs}) of 50fF.

With W=100μm and L = 0.16μm a parasitic capacitance of 50fF is obtained. The corresponding transconductance is: $g_{m1} = 14mS$

Next the optimal value for R_D has to be obtained. According to the expressions in table 5.4, the value of R_D is not of large influence on the TIA performance. Circuit simulations show that a value of 2kΩ yield best performance.

The maximal feedback resistance can be obtained by substituting the acquired values in the bandwidth expression from table 5.4: $R_f = 7.5k\Omega$. Circuit simulations however show that the 2GHz bandwidth can not be met because a second pole is present in the transfer function. Taking a smaller value, 2.5kΩ, is sufficient to meet the 2GHz requirement. The transimpedance of the TIA then is 2.2kΩ. All TIA values are listed in table 5.5

W	100μm
L	0.16μm
g_m	14mS
R_D	2kΩ
R_f	2.5kΩ
BW	2.1GHz
C_{in}	250fF
R_{TIA}	2.2kΩ

Table 5.5: TIA values

Sample-filter

The sample-filter is situated directly after the TIA (see figure 5.1). The task of this circuit is to select the appropriate part of each period and subsequently integrate the signal.

The sampling operation in the time-domain can be described by a mixing operation in the frequency-domain. After the mixing operation is performed, the wanted signal is situated at DC and the first unwanted component is situated at 80MHz. A low-pass filter should attenuate all unwanted harmonics for a large amount before the sampling operation of the ADC takes place. A sampling operation causes aliasing if the bandwidth of the unwanted components or noise is larger than half the sampling frequency and this should be prevented.

To reduce the noise bandwidth and to prevent aliasing the RC timeconstant should be sufficient high. However a large resistor and capacitor consume much silicon area. Because a high resolution matrix of receivers should be formed, this is not desirable: a trade-off between accuracy and area therefore have to be made.

According to [7] clock timing noise is transformed into amplitude noise by the slope of the signal, $\frac{\delta_v}{\delta_t}$,at that specific moment. The probability density function of timing noise, which is a Gaussian distribution, is multiplied with a scalar,in $\frac{\delta_v}{\delta_t}$, and resembles in a Gaussian noise function.

According to the figures in table D.1 a rms jitter value of <1ps is feasible. The maximal slope is approximately 16kV/s in the worst case situation which results in a maximal rms voltage noise, $\overline{v_{n.rms}} < 16nV$. This is negligible with respect to the to be measured signal.

The sampling jitter however also causes an integration area error due to variation in integration time. The analysis in appendix D.3 shows that a maximal peak-to-peak value of 5ps is feasible. Jitter can be described by phase-noise in the time domain. The phase-noise has a 1/f or $1/f^n$ behavior and therefore is situated at small offset-frequency of the fundamental frequency of the clock-signal. The sampling operation mixes also the phase noise to DC and is therefore situated at low-frequency. The low-frequency filtering operation therefore does not attenuate the phase-noise and thus the jitter contribution.

Amplifier

The information of the signal after the sampling operation is situated at DC. A hard requirement is that the amplifier should be highly linear. Each DC level should embrace exactly equal gain and therefore an OPAMP based amplifier is very suitable. It is already discussed that the noise contribution of the latter circuits in a chain are of minor influence. The signal information is however situated at DC and therefore a requirement is that the 1/f noise contribution is low. The amplification should be high enough such that the required ADC resolution is feasible.

ADC and DSP

The ADC should be shared for many (or all) receivers to limit the area consumption. Therefore to process the signals of all receivers, the sampling frequency of the ADC should equal the number of receivers multiplied with the required sampling frequency per receiver.

To prevent aliasing of the noise the sampling frequency for one receiver should exceed 2 times the bandwidth of the last analog receiver. For noise suppression the analog bandwidth is in the order of 50kHz → 100kHz (see section 5.1.2), which allows sharing a typical ADC for many pixels. The required ADC should be higher than about 10b.

5.1.2 Performances

The accuracy of the measurement of τ is mainly limited by timing errors, device noise, non-linearity errors and bandwidth limitations. In this section it is investigated first to what extend the non-linearity influences the measurement by numerical analysis and subsequently the amount of noise contribution and distribution is estimated with circuit simulations. At last it is estimated to what extend the τ accuracy is influenced by all the circuit limitations and what matrix resolution is feasible.

non-linearity simulations:

In appendix F it is described that non-linearity components appear at frequencies that are used to estimate τ due to intermodulation between the independent frequency components of the input signal. A circuit simulation is performed to obtain the influence of the non-linearity products on the τ measurement. A sinus signal is placed at the input of the TIA and the higher order output harmonics are obtained and reflected in table 5.6. The input current is

I_{in} (μA)	$h_1(V)$	$h_2(V)$	$h_3(V)$
0.01	19.2 μ	73.1p	76.1p
0.1	192 μ	212p	517.9p
1	1.92 m	55.01n	4.92n
10	19.2m	5.92μ	163n

Table 5.6: Frequency components introduced due to non-linearity of the mixer

in the range of several nano-amperes till several micro-amperes and the resulting magnitude of the second and third order components reflected in table 5.4 are negligible with respect to the magnitude of the fundamental component. Therefore it can be concluded that non-linearity of the TIA has a very minor effect on the system performance.

Noise simulations:

The receiver should be designed such that with almost all measurements (approximately 99%) the required accuracy is obtained. Therefore a worst case

magnitude error (which can be positive or negative) that is bigger than 99% of all noise values has to be chosen.

Noise has a Gaussian distribution and therefore about 99.7% of all noise errors are within three standard deviation (3σ) away from the mean value. One standard deviation of noise is equal to the root mean square noise value:

$$\sigma_{v_n} = \overline{v_{n.rms}}$$

and the rms noise value is equal to the square of the integrated noise power density spectrum:

$$\overline{v_{n.rms}} = \sqrt{\int_0^\infty \overline{v_n^2} df}$$

Therefore three times the rms noise value is taken as maximal magnitude error.

A circuit simulation is performed to obtain the noise contribution and distribution. The resultant noise distribution is shown in table 5.7. A non optimized

	Total noise(%)	ex. OPAMP
Phote Diode	0.0%	0.0%
TIA 1/f noise	23.3%	59.7%
TIA thermal noise	0.5%	1.3%
RC-filter	15.2%	39.0%
OPAMP	61.0%	-

Table 5.7: Error distribution

OPAMP based amplifier is implemented and this design dominates the total noise contribution (61%). The optimization of the OPAMP design falls out of the scope of this thesis. It can however be assumed that the noise contribution can be limited significantly. The noise distribution without the OPAMP taken into account is shown in the third column of table 5.7 and shows that the 1/f noise of the TIA and the thermal noise of the RC-filter dominate the total noise contribution.

The square of total integrated output noise power (rms noise voltage)is equal to 2.2mV. The worst case magnitude error therefore becomes ±6.6mV.

The ADC error contribution is small and not taken into account further on.

τ Accuracy and feasible resolution

First the optimal timing values have to be obtained to acquire a maximal accuracy. It is shown in table 5.1 and 5.2 that the situation with t_1 =1.0ns results a larger τ error than with t_1 =1.5ns for a BW of 2GHz. The allowed magnitude error however decreases with a larger value for t_1 according to the figures in table 5.3. A circuit simulation results a maximal τ error of 14ps due to a limited bandwidth of 2GHz for both cases (t_1 =1.0ns and t_1 =1.5ns). According to the figures in table 5.1 and 5.2, which is a reflection of a numerical

analysis, this was not expected. In the numerical analysis a first order transfer for the TIA was used that does not fully correspond with the circuit analysis, which shows a second order transfer. Therefore the difference is obtained.

From the above analysis it can be concluded that t_1 =1.0ns results in best performance and therefore this situation is worked out in detail.

The optimal timing values to obtain maximal accuracy are obtained with a numerical analysis and are reflected in table 5.8.

t_1	1ns
t_2	2ns
t_3	5.6ns
t_4	6.6ns

Table 5.8: Optimal timing values

The goal of this section is to obtain the required optical input power level for a maximal τ measurement error of 50ps for all cases. It is shown in appendix D.3 that maximal measurement errors occur for τ=1ns or τ=10ns. Circuit simulations were done to both estimate the output signals V_{OUT1} and V_{OUT2} (see figure 5.1) that are used to estimate τ, and to estimate the noise levels therein.

The simulation results are shown in table 5.9. The simulated values contain errors introduced due to bandwidth limitations and timing errors.

	$\tau = 1ns$	$\tau = 10ns$
V_{OUT1}	58.153m	268.566m
V_{OUT2}	0.552m	169.786m
$3{\cdot}\sigma_{v_n}$	6.6mV	6.6mV
ε_τ	1.8ns	5.9ns

Table 5.9: Simulated average area's, $3{\cdot}\sigma_{v_n}$ and corresponding τ error

In appendix **??** the expression to acquire the τ value, inclusive magnitude errors, is derived:

$$\tau_\epsilon = -\frac{t_3 - t_1}{ln\left(\frac{V_{OUT2}+3{\cdot}\sigma_{v_n}}{V_{OUT1}+3{\cdot}\sigma_{v_n}}\right)} \tag{5.4}$$

Substituting the simulated values (shown in table 5.9) in (5.4) yields the τ errors shown in the last column of table 5.9.

Numerical analysis show that for a maximum τ error equal to 50ps minimal input current of 75μA is required for this circuit. With an optical power to current transfer of the photo diode of minimal 0.12A/W this results in a minimal needed input power of 625μW. The delivered optical input power is 50μW per sample and therefore this circuit is not feasible for this application.

In chapter 6 the circuit and system are optimized leading to a significant reduction in required optical power.

5.2 Frequency sampling method

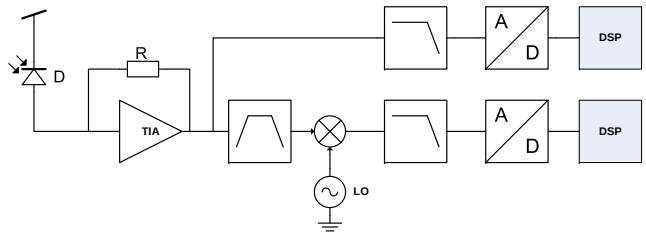

Figure 5.4: System of Frequency Sample method

The system of the *Two Frequency sample method* is shown in figure 5.4 and the frequency behavior of the received signal is shown in figure 5.5. In chapter 3 it is described that measuring the magnitudes of two independent frequency components is sufficient to extract the value of τ of the received signal. This value can be derived by substituting the measured magnitudes in expression D.37. In section D.3 the maximal allowed magnitude errors to meet the formulated specifications are derived. In this section the practical limitations and feasible performances are investigated.

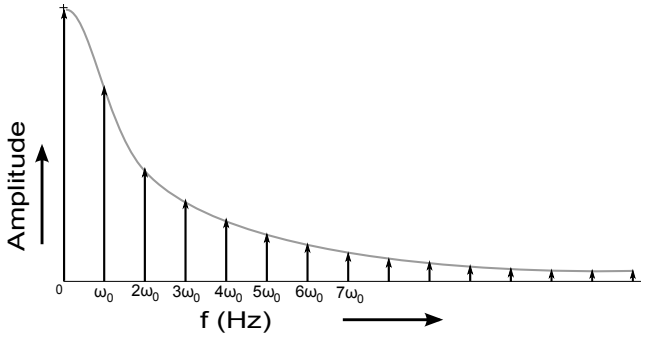

Figure 5.5: Frequency description of the received signal

5.2.1 System properties

The most important design constraints are listed

- Best performance with measurement of DC component (which suffers from 1/f noise)
- Non-linearity causes intermodulation of the individual components
- Mixing to DC yields the real or complex part of the signal.
- Limited bandwidth needed (160MHz)

Table D.2 shows that the measurement of the independent frequency component situated at DC in combination with the component situated at 160MHz yields best accuracy. A disadvantage of measuring the DC component is that any 1/f noise introduced is situated around 0 Hz.

In appendix F it is described that non-linearity components appear at frequencies that are used to estimate τ due to intermodulation between all independent frequency components of the input signal. A circuit simulation is performed in section 5.2.2 to obtain the influence of the non-linearity products on the τ measurement.

The DC component does not have to be mixed and therefore only suffers from non-linearity of the amplifier. A difficulty while measuring the DC component and the 160MHz component is that the gain of both paths is not identical. Therefore to not introduce a big error, the exact gains of both paths has to be measured in a calibration phase.

Another drawback of the system is that the a complex component must be measured. To measure the magnitude of the complex signal, the component should be mixed with a complex (sine) and a real(cosine) LO signal. A phase error however degrades the measurement accuracy. Also two branches are needed or two sequential measurements has to be performed. Both possibility has its disadvantages. This influence and the influence of the phase error is however investigated at last.

5.2.2 Circuit design

Figure 5.4 shows the system of the frequency sample method. The system consists of an I-V converter, two filters, a mixer and an ADC. The circuits should satisfy the listed specifications

- Bandwidth of first amplifier larger than 160MHz
- Highly linear circuits (amplifiers and especially mixer)
- Low 1/f noise

The design challenges of each circuit are now described.

Amplifier

According to the FRIIS noise equation [5] the first stages of the receiver should have a maximal gain and minimal noise contribution to achieve an optimal noise performance. However to obtain a receiver that suffers minimal from non-linearities, the first stages should have a minimal gain and the linearity requirement for the last stages is highest. Because of this contradiction, there is no optimum for both requirements.

The non-linearity requirement is very strict. Therefore an amplifier with resistive feedback is used. The advantage of a feedback amplifier is that the circuit can be perfectly linear if the open loop gain of the amplifier is infinite.

This is however never the case and therefore a small degradation in linearity is obtained.

In most mixer designs the input signal is presented as gate voltage of a tail current source of a differential pair. Therefore the amplifier can be performed as a current amplifier. A standard high gain current amplifier is shown in figure 5.6

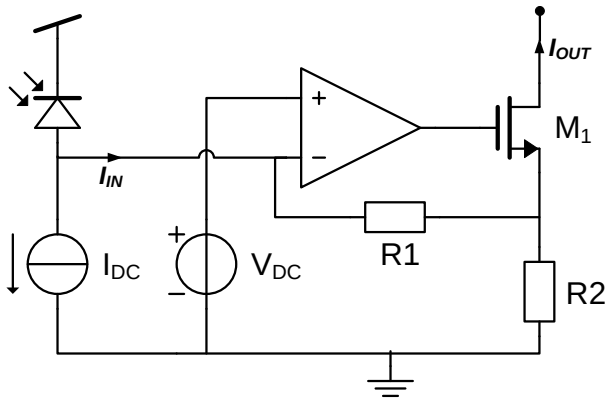

Figure 5.6: General OPAMP bases current amplifier

Mixer

There are basically three classifications for mixers:

- Unbalanced; single-ended input and output.
- Single balanced; differential design except single-ended input.
- Double balanced; fully differential.

The down-conversion unbalanced mixer generates an IF output consisting of f_{in}, f_{LO}, f_{in}-f_{LO}, f_{in}+f_{LO} and other spurious products. Single balanced mixers output the same frequency components but strongly attenuates either the input signal or the LO signal. Double balanced mixers only outputs the sum and difference frequency of the input and LO signal. Due to its fully differential design, it also suppresses the even distortion products.

In this research the desired component is mixed to DC and therefore no unwanted DC products should be outputted by the mixer. The unbalanced mixer outputs also the original input signal, which contains also a DC component, and is therefore not suitable for this application.

The double balanced mixer requires a differential input signal. The input signal for this application is however single-ended and therefore a balun circuit is required to generate the differential signal. This introduces extra noise and nonlinearity and this is not wanted. Because of these reasons the single balanced mixer is most suitable for this application.

Most mixers are performed as hard-switching multipliers. This means that the LO signal is shaped as a square wave. In this case the LO signal can be generated by digital circuits and the noise, linearity and gain performances exceed the performance of the use of a sinusoid LO signal. A disadvantage of a square wave LO signal is that its frequency spectrum contains the fundamental frequency component and a component at every odd harmonic. In our case these harmonics are exactly situated at corresponding frequency components of the received signals. This results mixing of these unwanted products to DC. Therefore a very 'clean' sinusoid LO signal is required.

Circuit simulations

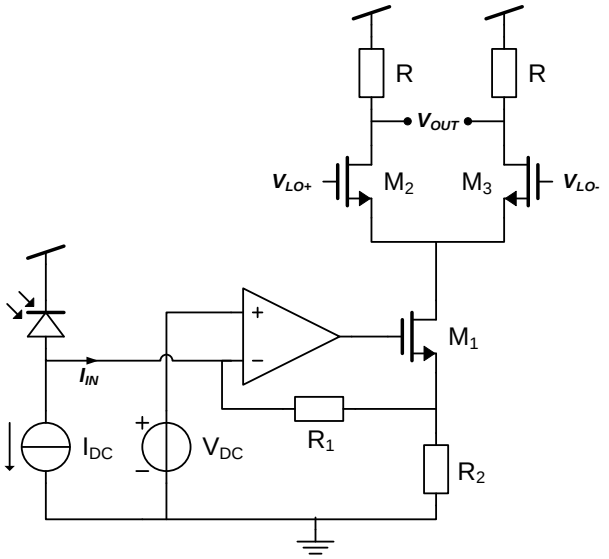

Figure 5.7: Amplifier and mixer circuit

Circuits simulations are performed with the circuit shown in figure 5.7. It is already described that the non-linearity of the circuit is a big problem for this method. Therefore a non-linearity analysis is performed first with an ideal amplifier but with a non-ideal (and thus non-linear) single balanced mixer.

Influence of non-linearity:

The input current and the LO voltage both show a non-linear propagation path to the output. Therefore the influence of non-linear behavior on both signals is investigated. First a circuit simulation is performed with constant tail current and a variable LO voltage. The results are shown in table 5.10. The results of the circuit simulation shows that a large V_{LO} results in a large third order component. Because the input signal contains a frequency component at each harmonic of the fundamental frequency, which is equal to the LO frequency, the non-linearity components of the LO will mix unwanted components of the

V_{LO}	$H_1(V)$	$H_2(V)$	$H_3(V)$
0.1m	0.22m	0.9p	0.9p
1m	2.2m	8.9n	22n
10m	22m	57n	30μ
100m	280m	260n	15m

Table 5.10: Frequency components introduced due to non-linearity propagation of V_{LO}

input signal to DC. To reduce the influence of this effect, the LO magnitude may not exceed 10mV.

Next a circuit simulation is performed to obtain the influence of non-linearity of the mixer on the input signal. A sinusoid current with variable amplitude is putted on the input of the current amplifier. The results of the simulation are shown in table 5.11. The figures in table 5.11 show that that the second

I_{in}	$H_1(V)$	$H_2(V)$	$H_3(V)$
1n	6.95μ	1.40n	0.1p
10n	69.5μ	140n	100p
100n	695μ	14.0μ	100n
1μ	7.9m	1.50m	117μ

Table 5.11: Frequency components introduced due to non-linearity propagation of I_{IN}

order components are much higher with this input range than the third order components. The second order and third order coefficients can be derived with:
$\alpha_2 = \frac{2\,V_{out2}}{V_{out1}^2} = 58$
$\alpha_3 = \frac{4\,V_{out2}}{V_{out1}^3} = 1.7 \cdot 10^6$

A algebraical analysis is performed with the obtained non-linearity coefficients to acquire the total error components at frequencies used to estimate τ. The results are shown in table 5.12. This analysis shows that this method is only

F_0 (nA)	τ error
1	1.7ps
10	8.4ps
100	84ps
1000	850ps

Table 5.12: τ errors introduced due to non-linearity of the mixer with variable input current

feasible for very small input currents while taking only the non-linearity into account. The noise contribution however makes a accurate measurement with very small input currents impossible for this method.

Chapter 6

System and Circuit Optimization

In chapter 5 the *average area measurement* and *frequency sampling* method are worked out in detail at a circuit design level implementation point of view. It is shown that the *frequency sampling method* is not feasible for this application because the required accuracy can not be met. The 'average area measurement' method can meet the accuracy requirement however the required resolution is by far not feasible. In chapter 2 it is described that a maximal optical power of 5nW can be delivered per pixel for cell imaging. With an optical power to current transfer for the photo diode of minimal 0.12A/W (which is described in 5.1.1) one receiver should be capable to meet the required accuracy with an input current for F_0 of 0.6nA to be suitable for cell imaging.

6.1 Average area method

The system of the Average area method is shown in figure 6.1. In chapter

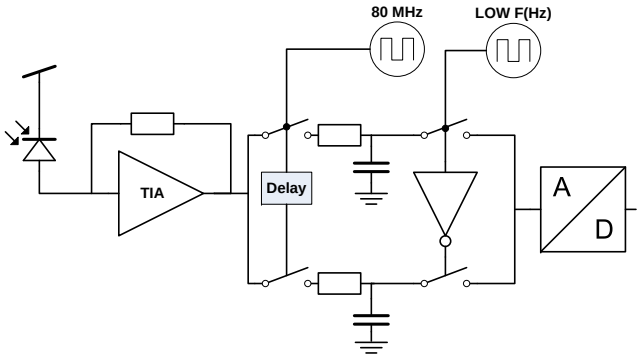

Figure 6.1: System of *Two average area method*

5.1.2 it is obtained that an input current for F_0 of 75μA is required to meet the accuracy requirement. The figures in table 5.5 show that the OPAMP, the $1/f$ noise contribution of the TIA and the kT/C noise contributed by the RC sampling filter are the main noise contributors to inaccuracy. In this chapter

multiple optimizations are introduced to reduce the influence of these dominant contributors.

6.1.1 3 branches

The noise contribution of the TIA is correlated for both branches. Therefore this contribution can be seen as an variable added to the expression for each measurement. Adding a variable to the mathematical description described by (D.48) yields

$$AA(t_1, t_2) = \frac{-F_0 \cdot \tau}{1 - e^{-\frac{T}{\tau}}} \cdot \frac{e^{-\frac{t_2}{\tau}} - e^{-\frac{t_1}{\tau}}}{t_2 - t_1} + V_{TIA} \tag{6.1}$$

The expression now contains three variables and therefore three expressions (and thus measurements) are required to extract the value of τ. Solving the three expressions for τ yields

$$\tau = \frac{t_1 - t_3}{\ln\left(\frac{AA(t_3,t_4) - AA(t_5,t_6)}{AA(t_3,t_4) - AA(t_1,t_2)}\right)} \tag{6.2}$$

The mathematical accuracy can be obtained by performing the same steps as described in appendix **??**. Doing so, the accuracy decreases with a factor 7 with respect to the measurement of two areas.

6.1.2 TIA Chopping

The TIA noise contribution is mainly dominated by $1/f$ noise. The ratio between the 1/f noise contribution (integrated from 100Hz - 1GHz) and the thermal noise contribution (integrated from 0Hz - 1GHz) is approximately 1:50. The influence of the low frequency noise can be reduced by modulating the low frequency noise to a higher frequency and unharm the input signal. This can be accomplished with a chopper circuit, which is shown in figure 6.2. The circuit contains of two additional multiplexers, an additional TIA and an adder. The input multiplexer connects the input of each TIA half a period to the photo diode and half a period to ground reference. The input current flows half a period through the upper TIA and the other half of the period through the lower TIA. The output multiplexer subsequently connects each TIA half a period to the plus input and half a period to the minus input of the adder. This causes that the input signal is constructed back to its original form at the plus input of the adder.

Both TIA's output a DC voltage that is equal to the low frequency content of their $1/f$ noise, this low frequency thermal noise and a constant DC level (respectively V_{DC1} and V_{DC2}). Because the output of both TIA's are toggled between the plus and the minus ports of the adder, the DC levels are in essence modulated with a square wave. This operation is shown in 6.2b. The low frequency components should be modulated at a frequency such that they will be filtered out before a sampling operation is performed at a lower frequency than half the modulation frequency to prevent aliasing. To unharm the signal

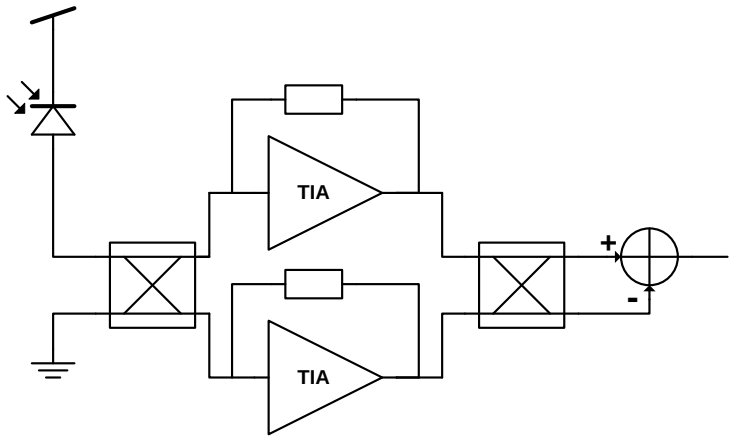

(a) Chopper Circuit

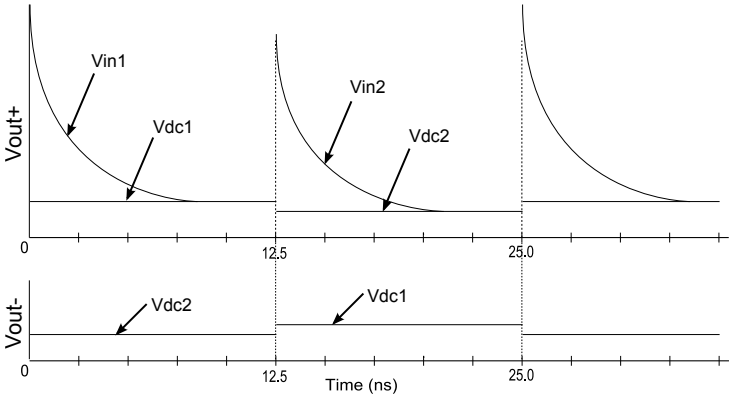

(b) Chopper time behavior

Figure 6.2: Chopper circuit a) and its time behavior b)

as much as possible a modulation frequency of half the fundamental frequency is taken (40MHz).

A square wave contains frequency components at all its frequency components and will therefore mix white noise presented around the odd harmonics (40,120,160.. MHz) generated by both TIA's to DC. The magnitude of the components however decreases with increasing amplitude (sinc form) and will therefore not introduce much additional thermal noise at low frequency.

Due to mismatches between both TIA's the transimpedance gain differs. This is however not of influence on the τ extraction as long as the gain for both samples is equal (which is the case with this modulation frequency).

6.1.3 Multiple-stage filtering

The kT/C noise contribution of the sampling RC filter is significantly large in the circuit described in chapter 5.1. This can be reduced by performing the sampling and filtering in multiple stages. It is already described that after the

sampling operation, the relevant information is located at DC. The spectrum however still contains (unwanted) frequency components at all integer multiples of the fundamental frequency and contains noise spread over a large bandwidth of the spectrum. To prevent aliasing, the unwanted frequency components and noise should be filtered before the analog to digital conversion is performed. It is however not required that the filtering is performed directly after the sampling: to reduce the influence of the kT/C noise of the filter the sampled signal can be amplified first. This reduces the kT/C contribution with a factor A^2 (where A is the gain of the amplifier). This operation is shown in figure 6.3

To reduce the total noise contribution the bandwidth of the filter should be as low as possible. In the analog domain this however requires a large capacitor and resistor value, which consumes much silicon area. This is not wanted because a high resolution matrix should be formed. The filtering operation can also be performed in the digital domain. Then the only requirement for the filtering in the analog domain is that aliasing is prevented. This requires that the filter bandwidth is smaller than $\frac{1}{2}Fs$. To limit the area consumption of this

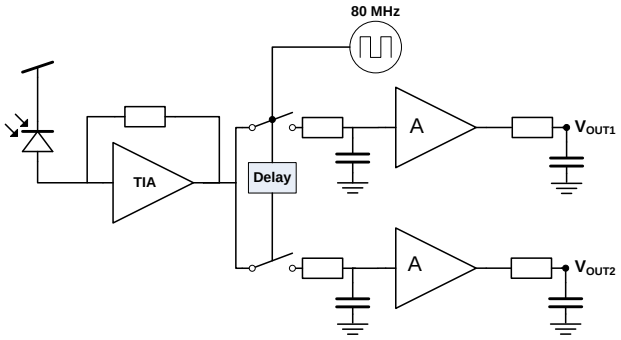

Figure 6.3: Time averaging system with multi stage sampling and filtering

analog filter, the maximal capacitance is set to 10ps and the resistance is set to 10kΩ. The bandwidth then is: $BW = \frac{1}{2\pi RC} = 1.6MHz$ and therefore the the sampling frequency per receiver should be higher than about 4MHz. For this sampling frequency a typical ADC can be shared between many pixels. The minimal bandwidth of the extern digital filter is only limited by the available measuring time.

6.1.4 Performance

In this section the performance of the optimized circuits for the *Average Area Method* with respect to noise are compared with the circuit designed in chapter 5.1. Subsequently the required optical input power level for a maximal τ measurement error of 50ps for all cases is obtained for the optimized circuit. Circuit simulations were done to both estimate the output signals V_{OUT1} and V_{OUT2} (see figure 6.2) that are used to estimate τ, and to estimate the noise levels.

Furthermore the influence of less strict requirements, longer measurement time and larger allowed τ error, on the feasible optical resolution is obtained.

	Standard		2 stage sample/filtering		Chopping + 2 stage s/f	
	$\overline{v_{n.tot}^2}$	%	$\overline{v_{n.tot}^2}$	%	$\overline{v_{n.tot}^2}$	%
TIA 1/f	$11.4{\cdot}10^{-5}$	55	$11.4{\cdot}10^{-5}$	97.2	$5{\cdot}10^{-9}$	0.0
TIA therm.	$3.3{\cdot}10^{-6}$	1.5	$3.3{\cdot}10^{-6}$	2.8	$2.4\cdot10^{-6}$	100
RC-sampler	$7.3{\cdot}10^{-5}$	35.4	$5.8{\cdot}10^{-9}$	0	$5.8{\cdot}10^{-9}$	0
OPAMP	$1.65\cdot10^{-5}$	8.1	0	0	0	0
$\overline{v_{n.tot}^2}$	0.2mV^2		0.12mV^2		$2.42\mu V^2$	
$\overline{v_{n.rms}}$	14mV		10.8mV		1.55mV	

Table 6.1: Noise Contributions of standard and optimized circuit

Noise circuit simulations are performed for three cases: for the circuit designed in section 5.1, the same circuit with the optimization described in section 6.1.3 and the same circuit with both the optimization described in section 6.1.2 and section 6.1.3 implemented. The simulation results show a significant decrease in noise contribution because of the implemented optimizations. The circuit simulations are performed with an ideal OPAMP. Performing a simulation with a non-ideal and non optimized OPAMP shows that the total noise contribution increases approximately 20%.

The figures in the last column of table 6.1 show that the noise contribution is by far dominated by the thermal noise of the TIA after implementing the optimization methods. Of this total noise 95% is contributed by the feedback resistance. This noise contribution is a fundamental problem and can not be lowered by component optimization without reducing the transimpedance gain. The only possibility to reduce the total noise contribution is to reduce the bandwidth of the filter. The minimal bandwidth is however also limited by the available measuring time, which is limited to 1ms to prevent bleaching of the cells.

The output signals V_{OUT1} and V_{OUT2} (see figure 6.2) that are used to estimate τ, are shown in table 6.2. These simulated values contain errors introduced due to bandwidth limitations and timing errors. The measured values are obtained an input current leading to F_0 =0.1μ. In chapter 5.1.2 it is described that

	$\tau = 1ns$	$\tau = 10ns$
V_{OUT1}	58.971mV	271.087mV
V_{OUT2}	0.585mV	171.316mV
$3{\cdot}\overline{v_{n.rms}}$	4.65mV	4.65mV
$\tau_{varepsilon}$	0.95ns	1.10ns

Table 6.2: Measured average area's, $3{\cdot}\overline{v_{n.rms}}$ and corresponding τ error

$3\cdot\overline{v_{n.rms}}$ is taken as maximal magnitude error. Substituting the output signals V_{OUT1} and V_{OUT2} shown in table 6.2 in expression 5.4 gives the τ measurement error which is shown in the last row of this table.

Numerical analysis show that for a maximum τ error equal to 50ps minimal input current of 3.7μA is required for this circuit. With an optical power

to current transfer of the photo diode of minimal 0.12A/W this results in a minimal needed input power of 37μW. The delivered optical input power is 50μW per sample and therefore this circuit is capable to image one pixel.

Influence of a longer allowed measurement time:

If a longer measurement time than 1ms is allowed, the signal can be averaged (or filtered) over a longer period which results in a smaller noise contribution. The rms noise voltage reduces with $\sqrt{n}$ where n equals the numbers of samples. A circuit simulation is performed to obtain the influence of a longer measurement time on the noise contribution. Also a numerical simulation is performed to obtain the minimal required optical input power level for a maximal τ measurement error of 50ps for all cases. The results are shown in table 6.3.

Meas. time	$\overline{v_n^2}$	$\overline{v_{n.rms}}$	$P_{min}(\mu$ W)	#pixels
100μs	52.4μ	7.2m	150	0
1ms	5.28μ	2.3m	48	1
10ms	0.524μ	0.72m	15	3
100ms	51.9n	0.23m	4.8	10
1s	4.67n	0.072m	1.5	32

Table 6.3: Integrated noise contribution and corresponding feasible resolution for variable settling time

Influence of larger allowed τ error:

The influence of a larger allowed τ error is obtained performing an algebraical analysis and the results are shown in table 6.4. From the analysis results shown

	Meas. time = 1 ms		Meas. time = 100 ms	
τ error	P_{min} (μW)	#pixels	P_{min} (μW)	#pixels
50ns	48	1	4.8	10
100ns	18.3	2	1.83	27
200ns	8.8	5	0.88	56
300ns	5.3	9	0.53	94
400ns	3.7	13	0.37	135
500ns	2.8	17	0.28	178

Table 6.4: Minimal needed optical power and feasible resolution with respect to variable τ error

in table 6.3 and 6.4 it can be seen that with relaxed requirements (settling time and τ resolution) the feasible resolution is increased largely.

Chapter 7

Conclusion and Recommendations

This thesis presents the analysis and design of an integrated optical receiver for *Fluorescence Lifetime Imaging Microscopy*. A receiver, which performs the measurement for one pixel, is designed and is targeted to process the very low power optical signal to a digital value that corresponds to a unique lifetime (τ) of a molecule. The aim is to produce a high resolution image for Cell imaging, for which a high resolution matrix (both spatial and in time accuracy) of receivers is required. The main challenge is to design a very low noise and low area consuming receiver.

The received signal is quantified and multiple methods to extract τ are mathematically analyzed. Two most suitable methods from a mathematical point of view,the 'Average Area Method' and the 'Frequency sample method', are worked out in detail at circuit level.

The circuit non-idealities and the corresponding influence on the accuracy of the measurement are obtained for both methods. It is shown that the 'Frequency sample method' cannot meet the accuracy requirements for the available optical input power density. A straight forward implementation of the 'Average area method' can meet the accuracy requirements but only for a very low spatial resolution. Introducing a number of accuracy increasing measures into the 'Average area method' increases the spatial resolution by a few orders of magnitude.

The main noise contributors of the circuit for the 'Average Area Method' are the TIA 1/f noise and the kT/C noise of the RC-sampling filter. The influence of these noise sources is reduced with the implementation of two methods. A 'chopper circuit' is implemented to modulate the dominating 1/f noise to a higher frequency that is attenuated by a low-pass filter afterwards. Secondly the filtering is performed after the sampled signal is amplified; the kT/C noise is reduced with factor A^2.

The implementation of both methods yields an rms noise reduction of approximately a factor 10, but the required accuracy of the measurement is still not acquired by far for the available very low optical power. Therefore the feasible resolution is much lower than the required resolution for Cell imaging.

The feasible resolution can be increased by taking less strict requirements; longer measurement time and larger allowed τ error.

Most fluorescence samples display more than one exponential decay and therefore contain multiple lifetimes. The investigated methods are not suitable to extract the relevant data from the multi-exponential data. The methods however can be expanded to become suitable for this occurrence. A brief explanation is described in appendix B.

7.1 Recommendations

As described above,t the investigated methods are not suitable to extract multiple τ values from samples with a multi-exponential decay. In appendix B a method is described, which is used in many FLIM applications, that uses a curve fitting algorithm to approximate the emitted (multi-) exponential curve and estimates the corresponding (multiple) Fluorescence Lifetime(s). Further research in this area is preferred to obtain the performances of a combination of the designed circuits with the curve fitting algorithm. A small adaption to the designed circuit for the 'Average Area Method' is sufficient to make the circuit suitable to combine with the fitting algorithm. This is described in appendix B.

In this thesis the time domain variant of FLIM is investigated. Frequency domain FLIM is described in appendix A and further research on the feasibility of the implementation of this method is preferred.

Appendix A

Frequency domain FLIM

The fluorescence lifetime can be measured in two ways: by a time domain method that uses a periodic pulse excitation signal and by a frequency domain method. The frequency domain method excites the sample by a sine-wave and a DC component. Due to the decay of lifetime emission, the emitted light will show a phase-shift and a decrease in modulation dept. This is shown in figure A.1 for respectively a long and short lifetime. The lifetime can be measured

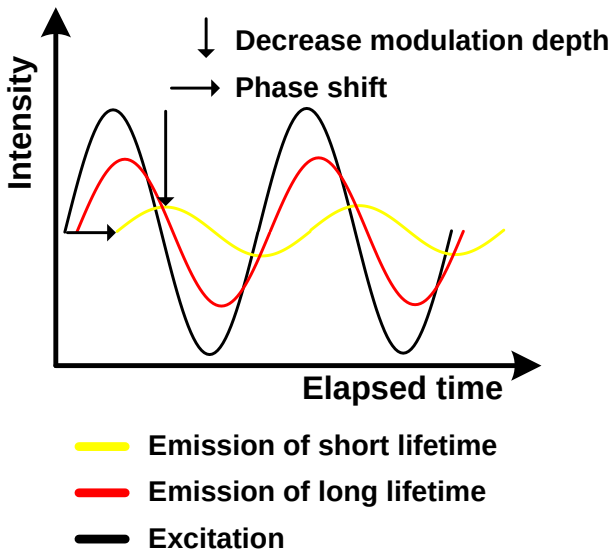

Figure A.1: Frequency domain FLIM

from each of these two parameters by the expressions:

$$\tau_\phi = \frac{\tan(\phi)}{\omega} \tag{A.1}$$

where ϕ equals the phase delay between the excitation sine and the emitted sine, and

$$\tau_m = \frac{1}{\omega}\sqrt{\frac{1}{m^2} - 1} \tag{A.2}$$

where 'm' equals the ratio of the amplitude of the excitation sine divided be the excitation DC signal and the amplitude of the emitted sine divided by the emitted DC signal. This is described by

$$m = \frac{b/d}{a/c} \tag{A.3}$$

where 'a' is the amplitude of the excitation sine-wave, 'c' is excitation DC signal, 'b' is amplitude of modulated sine-wave and 'd' is the DC level of the modulated signal.

The extraction of τ by measuring the phase shift shows a great resemblance with the method described in appendix D.1.2, where τ extraction expression is described by (D.38). In this expression a_n and b_n correspond to the real and imaginary part of the emitted sin-wave and the ratio between b_n and a_n corresponds to $tan(\phi)$. Therefore the methods are mathematical similar and the same accuracy requirement and properties hold for these methods. In appendix D.3 it is described that the required accuracy is not feasible for the method described in appendix D.1.2 and therefore this frequency domain method, measurement of the phase shift, is also not feasible with the obtained timing error.

The extraction of τ by the decrease in modulation depth described by (A.2) and the frequency domain signal generated by a periodic pulse which is described in appendix D.1.2 also show a great similarity. In appendix D.1.2 the sample is excited with frequency components with equal magnitude. Substituting an equal value for 'a' and 'c' in (A.2) and (A.3) results the exact same expression as the τ extraction expression described by (D.37) with $\omega_1 = 0$ Hz. Therefore the same accuracy requirements and properties hold for these methods.

An advantage with respect to the frequency domain method described in appendix D.1.2 is that only a component at DC and ω result from the measurement. In chapter 5.2 it is described that the multiple frequency component introduce error components at critical frequencies due to non-linearity of the active circuits. With only a component present at DC and ω much less error components will appear due to non-linearity.

Appendix B

Multi-exponential decay and fitting algorithm

Most fluorescence samples display more than one exponential decay and therefore contain multiple uniique lifetimes(τ values). The intensity decay can be described by the multi-exponential model[8]:

$$I(t) = \sum_i \alpha_i e^{-t/\tau_i} \tag{B.1}$$

where i describes the number of decays, α the initial amplitude of each decay curve and τ_i the corresponding unique lifetime. The values of the variables α_i and τ_i can not be extracted from the sum of exponential functions algebraically. Conventional measurement methods use fitting algorithms like nonlinear least squares algorithms (NLLS)[8] to extract the unique values of α and τ. The NLLS algorithms are most used in studies.

Overview of Least-Squares Analysis[8]:

A least squares analysis starts with a model that is assumed to describe the data. The goal is to test whether the model is consistent with the data and to obtain the parameter values for the model that provide the best match between the measured data, N(t_k), and the calculated decay, $N_c(t_k)$, using assumed parameter values. This is accomplished by minimizing the goodness-of-fit parameter, which is given by

$$\chi^2 = \sum_{k=1}^{n} \frac{1}{\sigma_k^2}[N(t_k) - N_c(t_k)]^2 \tag{B.2}$$

In this expression the sum extends over the number (n) of data points used for a particular analysis and σ_k is the noise variance that should be known to optimize the fitting and can be measured with circuit simulation. Each value of $N(t_k)$ corresponds with its ideal value added with a mean value equal to $\pm\sigma_k$. Therefore if $N_c(t_k)$ corresponds to its ideal value, each summation contributes 1.0 to the value of χ^2. The optimal value for χ^2 is therefore equal to the number of data points.

During a NLLS analysis the values of α_i and τ_i of the multi-exponential model (B.1) are varied until χ^2 is a minimum. Examples of NLLS fitting algorithms are Gauss-Newton, modified Gauss-Newton and Nelder-Mead algorithms [9].

It can be derived that the more data points are measured, the higher the probability becomes that the calculated decay figure fits on the ideal value. This is because a property of random noise is that the probability that the mean deviation of the noise equals one σ approximates 100% if an infinite number of samples are taken. Therefore measuring more data points is equal to averaging noise and therefore this is in essence equal to a filtering operation.

Combination of fitting algorithm with the designed circuits

The average area circuit described in chapter 5.1 is optimized with respect to its noise contribution and can be adapted to be appropriate to combine with a fitting algorithm. It is described above that many data points per period results a minimal fitting error and thus τ error. To not set high bandwidth requirements for successive circuits it is not wanted to measure at a very high frequency. Therefore the sampling filter should integrate each period a slightly shifted period with respect to the previous period. This implies that the sampling frequency should be slightly smaller than the fundamental frequency of the input signal. A sampling frequency of for example 79.9MHz can be taken such that the fundamental signal is mixed to 0.1MHz and 800 samples are performed each period. The signal should however be mixed to an as small as possible frequency such that as much noise as possible can be 'filtered' before the fitting algorithm is performed. The minimal frequency is however limited by the maximal measurement time.

The fitting algorithms used to analyze the frequency domain data are analogous to those used for time-domain data. The frequency domain analysis described in appendix A should be performed at multiple excitation frequency such that a fitting algorithm can approximate the ideal frequency curve that is ideal for each (multiple) fluorescence decay.

Appendix C

Quantitative analysis

C.1 Time-domain Specifications

The time domain behavior of the the periodic signal can be described by the modulation of (1.1) at a frequency of 80MHz (in our case). This results in a periodic exponential function; a time domain plot of this periodic function is shown in figure C.1.

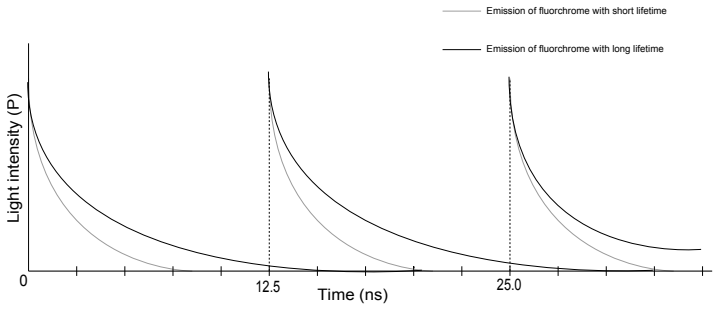

Figure C.1: Graphical representation of time-domain behavior of fluorescence emission at a repetition frequency of 80MHz

Most fluorophores commonly used in fluorescence microscopy have lifetimes (τ) ranging from 1 to 10 ns [3]. Because the time span of one period (12.5ns) does not exceed the maximal time constant (10ns) much, the emitted fluorescence of subsequent samples could overlap significantly. Therefore the exponential decay also affects the exact shape of the measured signal in the next periods (especially with large τ). As a result, the level of the signal in a certain period (N) is equal to the summation of the exponential function shifted with the period time (T) multiplied with the summation integer (k=0..(N-1)):

$$f_N(t) = \sum_{k=0}^{N-1} F_0 \cdot e^{-\frac{t+kT}{\tau}} \tag{C.1}$$

$$\Rightarrow f_N(t) = F_0 \cdot e^{-t/\tau} \sum_{k=0}^{N-1} \cdot e^{-\frac{kT}{\tau}} \tag{C.2}$$

The summation of the exponential function is a geometric series [1] and with $r = e^{-T/\tau}$ and $n = N$, a certain period N can be described by

$$f_N(t) = F_0 \cdot e^{-t/\tau} \cdot \frac{1 - e^{-\frac{T \cdot N}{\tau}}}{1 - e^{-T/\tau}} \tag{C.4}$$

for $0 \leq t \leq T$. This expression shows that the behavior of certain periods N_1 and N_2 differ with a factor $(e^{-\frac{T \cdot N_2}{\tau}} - e^{-\frac{T \cdot N_1}{\tau}})$. The ramp of the exponential function in the numerator of the fraction decreases with increasing $T \cdot N$ and approaches zero for $N \to \infty$.

For a limited "settling time" the error is sufficient small: for τ=10ns (worst case) the error in neglecting the $e^{-\frac{T \cdot N}{\tau}}$ term is only 0.19% for N=5. The situation when the effect of the $e^{-\frac{T \cdot N}{\tau}}$ term is negligible small will be denoted as (quasi) steady state. From now on it can be assumed that the real time measurement is performed in steady state and that the concerning exponential function in (C.4) thus can be neglected. This yields

$$f_p(t) = F_0 \cdot e^{-t/\tau} \cdot \frac{1}{1 - e^{-T/\tau}} \tag{C.5}$$

for each period.

C.2 Frequency-domain Specifications

The optical input signal can also be described in the frequency-domain. Describing the received signal algebraically in this domain enables the recovery of τ in this domain. The frequency behavior of the received signal can be obtained using the Fourier analysis. A property of the Fourier transform is that a convolution in time domain is equal to a multiplication in the frequency domain [10].

$$f(t) * g(t) = F(\omega) \cdot G(\omega) \tag{C.6}$$

Therefore to simplify the analysis, the optical input is modeled as a convolution of the exponential function and a periodic Dirac function (also known as a 'Dirac comb' or the 'Shah' function) with repetition frequency of 80 MHz. The Dirac comb is described by

$$g(t) = \sum_{n=0}^{\infty} \delta(t - n \cdot T) = \Delta_T. \tag{C.7}$$

[1] A series is geometric if for the series $\sum_k a_k$ the ratio of each two consecutive terms $\frac{a_{k+1}}{a_k}$ is a constant function of the summation index [9]. Because $\frac{e^{-(k+1)\frac{T}{\tau}}}{e^{-(k)\frac{T}{\tau}}} = e^{\frac{T}{\tau}}$, the summation of the exponential function is also a geometric series. A geometric series can be simplified to a constant function. For the general function $a_k = r^k$ this yields

$$S_n = \sum_{k=0}^{n} a_k = \frac{1 - r^{n+1}}{1 - r} \tag{C.3}$$

where T is the period-time ($\frac{1}{80MHz}$) and the exponential function is described by (2.1). The function g(t) is periodic and the function f(t) is non-periodic. A convolution of a periodic- and a non periodic-function is called a circular convolution which is described by (C.8). To convolute the periodic function with f(t), this function has to be integrated from zero to infinity while g(t) is integrated over one period. Therefore f(t) is replaced by a periodic extension of the function f(t). This periodic extension is described by a summation of f(t) shifted with one period (T) each summation.

$$(f * g)(t) = \int_0^T \left(\sum_{i=0}^{N} f(\tau + i \cdot T) \right) \cdot g(t - \tau)\, d\tau \tag{C.8}$$

In practice the measurement time is limited and positive. Therefore the summation of f(t)is lower limited by 0 and upper limited by $T \cdot N$ (where N denotes the number of periods). Figure C.2 shows (C.8) for τ=2ns and τ=10ns

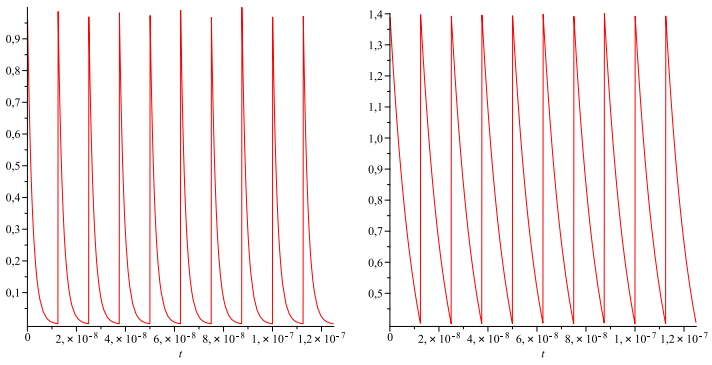

(a) Time-Domain (b) Time-Domain

Figure C.2: Convolution of 1.1 and C.7 with τ=2ns (a) and τ=10ns (b)

Because the received signal can be described by a convolution of two separate functions, the multiplication of the frequency behavior of each separate function yields the frequency behavior of the received periodic signal. Therefore first the frequency behavior of the separate functions has to be described. To obtain the frequency behavior of the exponential function a Fourier transform is taken from (1.1). The standard Fourier transform is shown in (C.9).

$$F(\omega) = \int_{-\infty}^{\infty} f(t) \cdot e^{-i\omega t}\, dt \tag{C.9}$$

The fluorescence measurement time is finite and positive; however it is assumed that the periodic function is in steady state during the real-time measurement. Therefore the integral is positive and unbounded. Substituting (1.1) in (C.9)

yields

$$F(\omega) = F_0 \cdot \int_0^\infty e^{-\frac{t}{\tau}} e^{-i\omega t}\, dt \tag{C.10}$$

$$= \frac{F_0}{\frac{1}{\tau} + i\omega} \tag{C.11}$$

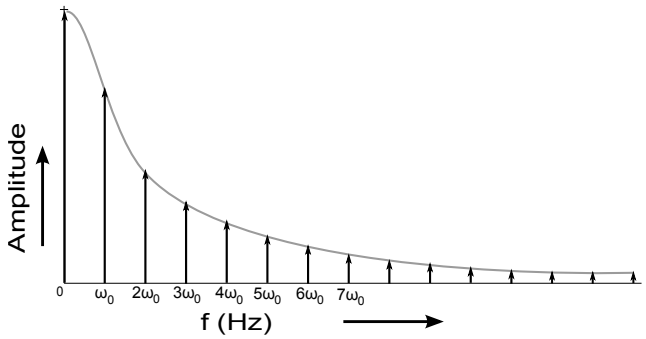

Figure C.3: Frequency behavior of (2.1)

The Fourier transform of the periodic dirac function yields:

$$G(\omega) = \int_{-\infty}^{\infty} (\sum_{n=0}^{N} \delta(t - n \cdot T)) e^{-i\omega t}\, dt \tag{C.12}$$

$$\Rightarrow G(\omega) = \frac{1}{T} \sum_{k=-\infty}^{\infty} \delta(f - \frac{k}{T}) \tag{C.13}$$

Expression (C.13) shows that the Fourier transform of the periodic dirac function results in a periodic dirac function in the frequency domain, with a period equal to $\frac{1}{T}$ (80 MHz). The $\frac{1}{T}$ before the summation shows that the dirac pulse is scaled by this factor. Because the amplitude of a dirac pulse is infinite, the amplitude in the frequency domain stays infinite. However the integral of a time-domain dirac pulse equals 1 therefore this value is thus scaled with a factor $\frac{1}{T}$ in the frequency-domain.

A convolution in the time domain corresponds to a multiplication in the frequency domain and therefore the frequency spectrums of the two separate functions F(t) and G(t) have to be multiplied with each other to get the frequency spectrum of (C.6). Multiplication with a dirac function corresponds with sampling at discrete times and therefore a sampled version of the frequency spectrum of the exponential function results. Because the periodic dirac function is scaled with a factor $\frac{1}{T}$, the exponential spectrum is also scaled with the same factor. The multiplication of the two functions yield

$$\begin{aligned} H(\omega) &= F(\omega) \cdot G(\omega) \\ &= \frac{F_0}{\frac{1}{\tau} + i\omega} \cdot \frac{1}{T} \sum_{k=-\infty}^{\infty} \delta(f - \frac{k}{T}) \end{aligned} \tag{C.14}$$

Expression C.14, with $F_0 = 1$ and $\tau = 2ns$, results the frequency domain plot given in figure C.3.

The frequency spectrum of the periodic exponential function described by (C.5) for one period can also be acquired by obtaining the Fourier coefficients of the periodic function. These Fourier coefficients describe a function in the frequency domain at integer multiples of the fundamental frequency ($\omega_0 = 2\pi/T$). Complex Fourier coefficients (c_n) describe the spectrum of a complex function and are therefore acquired. These complex Fourier coefficients of a general function f(t) are defined by [10]

$$c_n = \frac{1}{T} \int_{-T/2}^{T/2} f(t) e^{-in\omega_0 t} dt \tag{C.15}$$

The real time measurement only incorporates positive time and therefore the function (C.5) is integrated from 0 to T. This yields

$$\begin{aligned} c_n &= \frac{F_S \cdot F_0}{1 - e^{-T/\tau}} \int_0^T e^{-t/\tau} e^{-in\omega_0 t} dt \\ &= \frac{F_S \cdot F_0}{1 - e^{-T/\tau}} \cdot \frac{-1}{1/\tau + in\omega_0} \left[e^{-(1/\tau + in\pi)t} \right]_0^T \\ &= \frac{F_S \cdot F_0}{1 - e^{-T/\tau}} \cdot \frac{-1}{1/\tau + in\omega_0} \left(e^{-(T/\tau + in2\pi)} - 1 \right) \\ &= \frac{F_S \cdot F_0}{1 - e^{-T/\tau}} \cdot \frac{-1}{1/\tau + in\omega_0} \left(e^{-T/\tau} - 1 \right) \\ &= \frac{F_S \cdot F_0}{1/\tau + in\omega_0} \end{aligned} \tag{C.16}$$

Comparing (C.16) with (C.14) shows that both methods to determine the frequency behavior of the periodic exponential function are equal at the integer multiples of F_S. Therefore it can be concluded that both derivations are valid.

Appendix D

System design methods

D.1 Mathematical description of System design methods

D.1.1 Time-domain methods to extract τ

Three time-domain methods to extract τ from the received signal are described in this section. The measurement of two time-samples, two area measurements and a combination of a time-sample and an area measurement.

Extraction of τ: measurement of two time-samples

Equation (C.5) contains two unknown variables(τ and F_0), hence two independent values of f(t) at known t are required and sufficient to find the corresponding values for the concerned variables. Solving the two equations for τ yields:

$$e^{\frac{t_1-t_2}{\tau}} = \frac{f(t_2)}{f(t_1)}$$

$$\Rightarrow \tau = \frac{t_1 - t_2}{ln(\frac{f(t_2)}{f(t_1)})} \tag{D.1}$$

As figure D.1 shows one period of (C.5) for $\tau = 2$ns and $F_0 = 1$. Sampling at $t_1 = 0$ and $t_2 = 2ns$ and substituting $f_p t_1$ and $f_p t_2$ in (D.1)yields $\tau = 2.000$ns. Accuracy issues of this method are dealt with in section D.2.1.

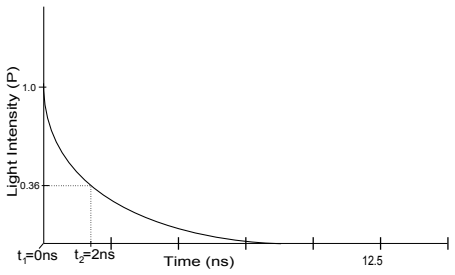

Figure D.1: Time-domain measurement at two time samples (t_1=0 and t_2=2ns) with $F_0 = 1$ and $\tau = 2ns$

Extraction of τ: two area measurements

Another method to extract the value of τ is to measure the area of the received signal over two separate periods. A requirement for the integration limits $\{t_1, t_2, t_3, t_4\}$ for each period is that the measurement results are independent. This is the case if the values of $\{t_1, t_2\}$ are not equal to the values of $\{t_3, t_4\}$. Integrating (C.5) from t=t_1 to t=t_2 yields

$$A(t_1, t_2) = \frac{-F_0 \cdot \tau}{1 - e^{-\frac{T}{\tau}}} \cdot (e^{-\frac{t_2}{\tau}} - e^{-\frac{t_1}{\tau}}) \tag{D.2}$$

Combining the equations for two measured areas A_1 and A_2 with integration limits $\{t_1, t_2, t_3, t_4\}$ yields

$$\frac{A(t_3, t_4)}{A(t_1, t_2)} = \frac{e^{-\frac{t_4}{\tau}} - e^{-\frac{t_3}{\tau}}}{e^{-\frac{t_2}{\tau}} - e^{-\frac{t_1}{\tau}}} \tag{D.3}$$

This function appears unsolvable for τ with arbitrary $\{t_1, t_2, t_3, t_4\}$. However specific values for $\{t_1, t_2, t_3, t_4\}$ give a function that is solvable. To find these values, the function can be simplified to

$$\frac{A(t_3, t_4)}{A(t_1, t_2)} = \frac{e^{-\frac{t_4}{\tau}} - e^{-\frac{t_3}{\tau}}}{e^{-\frac{t_2}{\tau}} - e^{-\frac{t_1}{\tau}}} = B \cdot \frac{e^{-\frac{t_2}{\tau}} - e^{-\frac{t_1}{\tau}}}{e^{-\frac{t_2}{\tau}} - e^{-\frac{t_1}{\tau}}} = B \tag{D.4}$$

The factor 'B' needs to meet two requirements. At first the factor should be solvable for τ. Second the multiplication of B with the latter fraction of (D.4) should result the first fraction. To meet the latter requirement, only exponential functions and additions of a constant value are allowed for this factor. To meet the first requirement, only one exponential function or one exponential function with an addition with the constant value are allowed. The allowed form for 'B' is restricted to

$$B_2 = e^{-\frac{C}{\tau}} + C_3. \tag{D.5}$$

To obtain this form, specific values for $\{t_1, t_2, t_3, t_4\}$ have to be taken. Inserting (D.5) for C_3=0 in (D.4) results in the expressions from which the conditions

for $\{t_1, t_2, t_3, t_4\}$ can be derived:

$$\frac{A(t_3,t_4)}{A(t_1,t_2)} = \frac{e^{-\frac{t_4}{\tau}} - e^{-\frac{t_3}{\tau}}}{e^{-\frac{t_2}{\tau}} - e^{-\frac{t_1}{\tau}}} = \frac{e^{-\frac{C_1}{\tau}} \cdot (e^{-\frac{t_2}{\tau}} - e^{-\frac{t_1}{\tau}})}{e^{-\frac{t_2}{\tau}} - e^{-\frac{t_1}{\tau}}} \tag{D.6}$$

$$\Rightarrow e^{-\frac{t_4}{\tau}} - e^{-\frac{t_3}{\tau}} = e^{-\frac{C_1}{\tau}} \cdot (e^{-\frac{t_2}{\tau}} - e^{-\frac{t_1}{\tau}}) \tag{D.7}$$

$$= e^{-\frac{t_2+C_1}{\tau}} - e^{-\frac{t_1+C_1}{\tau}} \tag{D.8}$$

The conditions for $\{t_1, t_2, t_3, t_4\}$ can now be derived for this case and are rendered in (D.10) and fig. D.2.

$$C_1 = t_4 - t_2 = t_3 - t_1 \tag{D.9}$$

$$\Rightarrow t_4 - t_3 = t_2 - t_1 = \Delta t \tag{D.10}$$

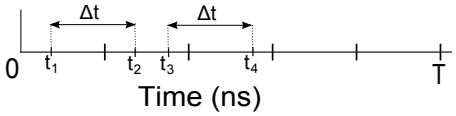

Figure D.2: Sample times

If these conditions are satisfied the function is solvable for τ and the factor 'B' is described by (D.5) with $C_3 = 0$.

Performing the previous steps for the substitution of (D.5) in (D.4) for $C_3 \neq 0$ yields:

$$\frac{A(t_3,t_4)}{A(t_1,t_2)} = \frac{e^{-\frac{t_4}{\tau}} - e^{-\frac{t_3}{\tau}}}{e^{-\frac{t_2}{\tau}} - e^{-\frac{t_1}{\tau}}} = \frac{e^{-\frac{t_2+C_2}{\tau}} - e^{-\frac{t_1+C_2}{\tau}} + C_3 \cdot e^{-\frac{t_2}{\tau}} - C_3 \cdot e^{-\frac{t_1}{\tau}}}{e^{-\frac{t_2}{\tau}} - e^{-\frac{t_1}{\tau}}} \tag{D.11}$$

The conditions that result from (D.11) are described by:

$$C_2 = t_4 - t_2 = t_2 - t_1 = \Delta t \tag{D.12}$$

$$t_3 = t_1 \tag{D.13}$$

$$C_3 = 1 \tag{D.14}$$

or

$$C_2 = t_3 - t_1 = t_2 - t_1 = \Delta t \tag{D.15}$$

$$t_2 = t_4 \tag{D.16}$$

$$C_3 = 1 \tag{D.17}$$

and visualized in fig. D.3 respectively fig. D.4.

If these conditions are satisfied, the function is solvable for τ and the factor 'B' is described by (D.5) with $C_3 = 1$.

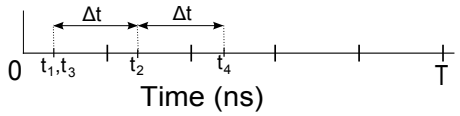

Figure D.3: Sample times

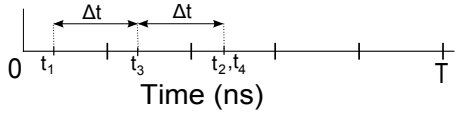

Figure D.4: Sample times

Solving (D.4) for τ, with (D.5) substituted yields:

$$\frac{A(t_3,t_4)}{A(t_1,t_2)} = e^{-\frac{C}{\tau}} + C_3 \tag{D.18}$$

$$\Rightarrow ln\left(\frac{A(t_3,t_4)}{A(t_1,t_2)} - C_3\right) = -\frac{C}{\tau} \tag{D.19}$$

$$\Rightarrow \tau = -\frac{C}{ln\left(\frac{A(t_3,t_4)}{A(t_1,t_2)} - C_3\right)} \tag{D.20}$$

Extraction of τ: two average area measurements

The extraction of τ by means of two average area measurements is a variant on the measurement of two areas method which is described in section D.1.1. The measured area is divided by the integration time, t_2-t_1, and yields

$$AA(t_1, t_2) = \frac{-F_0 \cdot \tau}{1 - e^{-\frac{T}{\tau}}} \cdot \frac{e^{-\frac{t_2}{\tau}} - e^{-\frac{t_1}{\tau}}}{t_2 - t_1} \tag{D.21}$$

The value of τ can be recovered performing two average area measurements. The same restrictions formulated in section D.1.1, which are described by (D.9-D.10) and (D.12-D.17), are applicable for this method. Performing the same steps as described in section D.1.1 to determine the expression to recover τ yields:

$$\tau = -\frac{C}{ln\left(\frac{AA(t_3,t_4)}{AA(t_1,t_2)} \cdot \frac{t_2 - t_1}{t_4 - t_3} - C_3\right)} \tag{D.22}$$

Extraction of τ: area measurement combined with a time-sample

Measurement of the area of one period(t=0..T) can be combined with the measurement of a certain time-sample to extract τ. Integrating (C.5) over one period results in the area of one period:

$$A(0,T) = \frac{-F_0 \cdot \tau}{1 - e^{-\frac{T}{\tau}}} \cdot (e^{-\frac{T}{\tau}} - 1) = F_0 \cdot \tau \tag{D.23}$$

Combining (C.5) with (D.23) results:

$$A(0,T) = \frac{\tau \cdot f(t_1) \cdot (1 - e^{-\frac{T}{\tau}})}{e^{-\frac{t_1}{\tau}}} \tag{D.24}$$

$$\frac{A(0,T)}{f(t_1)} = \frac{\tau \cdot (1 - e^{-\frac{T}{\tau}})}{e^{-\frac{t_1}{\tau}}} \tag{D.25}$$

Expression (D.25) shows that the wanted variable τ is present as a multiplication factor in the numerator and as power of the exponential functions; this function appears to be unsolvable algebraically. Therefore this function is probably not an option for the extraction of τ.

D.1.2 Frequency-domain methods to extract τ

Extraction of τ: measurement of two frequency-components

The frequency behavior of the received signal is shown in fig. C.3 and described by expression (C.14). These figures and expression show that the information to extract τ is hidden in the shape of the pulse train. This is described by (C.16).

Independent frequency components are only present at integer multiples of the modulation frequency F_S(80MHz in our case), the identification of the magnitude of a 2 components is required and sufficient to extract τ because expression (C.16) only incorporates two unknown variables (τ and F_0).

To obtain the magnitude of a complex function, the root of the squared imaginary and real part of the function has to be taken. The real and imaginary part of a function can be extracted using the complex conjugated of the function. The general formulas to obtain the imaginary and real part of an imaginary function are described by [10]:

$$Re(z) = \frac{(z + \bar{z})}{2}$$
$$Im(z) = \frac{(z - \bar{z})}{2i}$$

where $\bar{z}$ is the complex conjugated of a complex function z with z=a+ib and $\bar{z}$=a-ib. Elaborate the functions above with (C.16) yields the real part of the function

$$K_I(\omega) = \frac{\frac{1}{\tau}}{\left(\frac{1}{\tau}\right)^2 + \omega^2} \cdot F_0 \cdot F_S \tag{D.26}$$

and the complex part of the function

$$K_Q(\omega) = \frac{\omega}{\left(\frac{1}{\tau}\right)^2 + \omega^2} \cdot F_0 \cdot F_S. \tag{D.27}$$

The magnitude of K(ω) can be obtained by taking the root of (D.26) and (D.27) squared:

$$|K(\omega)| = \sqrt{\left(\frac{\frac{1}{\tau}}{\left(\frac{1}{\tau}\right)^2 + \omega^2}\right)^2 + \left(\frac{\omega}{\left(\frac{1}{\tau}\right)^2 + \omega^2}\right)^2} \cdot F_0 \cdot F_S \tag{D.28}$$

Solving these equations for τ with two magnitude measurements at $\omega = \omega_1 = n_1\,\omega_0$ and $\omega = \omega_2 = n_2\,\omega_0$ yields:

$$\left(\frac{|K(\omega_2)|}{|K(\omega_1)|}\right)^2 = \frac{\left(\frac{\frac{1}{\tau}}{\left(\frac{1}{\tau}\right)^2+\omega_2^2}\right)^2 + \left(\frac{\omega_2}{\left(\frac{1}{\tau}\right)^2+\omega_2^2}\right)^2}{\left(\frac{\frac{1}{\tau}}{\left(\frac{1}{\tau}\right)^2+\omega_1^2}\right)^2 + \left(\frac{\omega_1}{\left(\frac{1}{\tau}\right)^2+\omega_1^2}\right)^2}$$

$$\Rightarrow \left(\frac{|K(\omega_2)|}{|K(\omega_1)|}\right)^2 = \frac{\left(\frac{1}{\tau}\right)^2 + \omega_1^2}{\left(\frac{1}{\tau}\right)^2 + \omega_2^2}$$

$$\Rightarrow \tau = \sqrt{\frac{|K(\omega_2)|^2 - |K(\omega_1)|^2}{n_1^2\,\omega_0^2 \cdot |K(\omega_1)|^2 - |K(\omega_2)|\,n_2^2\,\omega_0^2}} \tag{D.29}$$

The value of τ can also be abstracted measuring only the real or only the complex parts of each individual frequency component. This corresponding expressions can be derived from respectively expression D.26 and D.27. This yields respectively

$$\tau = \sqrt{\frac{K_I(\omega_2) - K_I(\omega_1)}{n_1^2\,\omega_0^2\,K_I(\omega_1) - K_I(\omega_2)\,n_2^2\,\omega_0^2}} \tag{D.30}$$

for the real components, and

$$\tau = \sqrt{\frac{K_Q(\omega_1)\,n_2 - K_Q(\omega_2)\,n_1}{\omega_0\,(n_1\,n_2^2\,K_Q(\omega_2) - n_2\,n_1^2\,K_Q(\omega_1))}} \tag{D.31}$$

for the complex components.

Extraction of τ: I and Q frequency measurement

The received signal contains an imaginary and a real part in the frequency domain. Therefore the measurement of these individual parts is also a method to extract τ from the received signal.

A periodic signal can be presented as a linear function of the basic functions $\cos(n\omega_0 t)$ and $\sin(n\omega_0 t)$ by describing the function as a Fourier series [10]:

$$f(t) = \sum_{n=0}^{\infty} a_n \cos(n\omega_0 t) + b_n \sin(nt\omega_0 t)$$

Here a_n and b_n are the fourier coefficients and represent the amplitude spectrum at all integer multiples of the fundamental frequency (ω_0) of respectively the real and the imaginary part. The amplitude of one peak at a integer multiple of the fundamental frequency is thus described by

$$f_n(t) = a_n \cos(n\omega_0 t) + b_n \sin(nt\omega_0 t)$$

This expression shows large correspondence with a quadrature amplitude modulated (QAM) signal [5] described by

$$x(t) = I(t)\cos(\omega_0 t) + Q(t)\sin(\omega_0 t)$$

where a_n and b_n are replaced respectively by I(t) and Q(t). With quadrature amplitude demodulation, the modulated signal is multiplied with $\cos(n\omega_0 t)$ and $\sin(n\omega_0 t)$ to acquire respectively I(t) and Q(t). Multiplying (D.1.2) with these signals yields respectively

$$f_I(t) = a_n \cos(n\omega_0 t)\cos(n\omega_0 t) + b_n \sin(n\omega_0 t)\cos(n\omega_0 t)$$

and

$$f_Q(t) = a_n \cos(n\omega_0 t)\sin(n\omega_0 t) + b_n \sin(nt\omega_0 t)\sin(n\omega_0 t)$$

Using standard trigonometric identities described in appendix E.1, this can be written as

$$\begin{aligned} f_I(t) &= \frac{1}{2}a_n[1 + \cos(2\omega_0 t) + \frac{1}{2}b_n \sin(2\omega_0 t)] \\ &= \frac{1}{2}a_n + \frac{1}{2}[a_n \cos(2\omega_0 t) + b_n \sin(2\omega_0 t)] \end{aligned} \tag{D.32}$$

and

$$f_Q(t) = \frac{1}{2}b_n + \frac{1}{2}[a_n \sin(2\omega_0 t) - b_n \cos(2\omega_0 t)] \tag{D.33}$$

Low-pass filtering these signals removes the high frequency terms (containing $2\omega_0 t$, leaving only respectively the a_n and b_n terms. These terms can be calculated with [10]

$$\frac{1}{2}a_n = \frac{1}{T}\int_0^T f(t)\cos(n\omega_0 t)\,dt \tag{D.34}$$

$$\frac{1}{2}b_n = \frac{1}{T}\int_0^T f(t)\sin(n\omega_0 t)\,dt \tag{D.35}$$

substituting (C.5) in respectively (D.34) and (D.35) yields

$$f_I(t) = \frac{1}{2}a_n = \frac{F_S F_0 \tau}{1 + (n\omega_0\tau)^2} \tag{D.36}$$

$$f_Q(t) = \frac{1}{2}b_n = \frac{F_S F_0 \tau^2 n\omega_0}{1 + (n\omega_0\tau)^2} \tag{D.37}$$

The derivation of the last step is described in appendix .

Solving one of these functions for F_0 and combining the result with the other function results one function with only τ as unknown variable. Solving this function for τ yields:

$$\tau = \frac{b_n}{n\omega_0 a_n} \tag{D.38}$$

D.1.3 Combination of a frequency- and a time-domain method to extract τ

Extraction of τ: Area measurement combined with a frequency sample

The combination of a time-domain area measurement and the measurement of a frequency-domain sample is also an option. In previous subsection it was stated that expressions with τ present as power of an exponential function combined with τ as multiplication factor are not solvable for τ. Expression for area determination (D.2) shows minimal complexity with t_1=0ns and t_2=T and only contains τ as multiplication factor. In this case (D.2) can be simplified to

$$A(0,T) = F_0 \cdot \tau \tag{D.39}$$

Solving this function for F_0 and substituting this in the frequency-sample expression (D.28) yields

$$|K(\omega)| = \sqrt{\left(\frac{\frac{1}{\tau}}{\left(\frac{1}{\tau}\right)^2+\omega^2}\right)^2 + \left(\frac{\omega}{\left(\frac{1}{\tau}\right)^2+\omega^2}\right)^2} \cdot \frac{A(0,T)}{\tau} \cdot F_S \tag{D.40}$$

Solving this function for τ yields

$$\begin{aligned}
\left(\frac{|K(\omega)|}{F_S \cdot A(0,T)}\right)^2 &= \frac{\left(\frac{\frac{1}{\tau}}{\left(\frac{1}{\tau}\right)^2+\omega^2}\right)^2 + \left(\frac{\omega}{\left(\frac{1}{\tau}\right)^2+\omega^2}\right)^2}{\tau^2} \\
&= \frac{1}{(1+\omega^2\cdot\tau^2)^2} + \frac{\omega^2\cdot\tau^2}{(1+\omega^2\cdot\tau^2)^2} \\
&= \frac{1}{1+\omega^2\cdot\tau^2} \\
\Rightarrow \tau &= \sqrt{\frac{\left(\frac{F_S\cdot A(0,T)}{|K(\omega)|}\right)^2 - 1}{\omega^2}}
\end{aligned} \tag{D.41}$$

This however shows great resemblance with the τ expression for the two frequency samples method (D.37). It even appears that the expressions are equal when ω_1 equals 0Hz. This is logical because the DC component of the spectrum corresponds with the mean value of a signal which corresponds with the area divided by the area time. Because of this similarity, the accuracy of this method also equals the accuracy of the two frequency samples method. In the next chapter it has to be investigated which of the two methods is most practical to implement.

D.2 Accuracy of system design methods

D.2.1 Time-domain methods to extract τ

Extraction of τ: measurement of two time-samples

The τ-error of the measurement of two time-samples is affected by timing- and magnitude-errors; this is reflected in figure D.5.

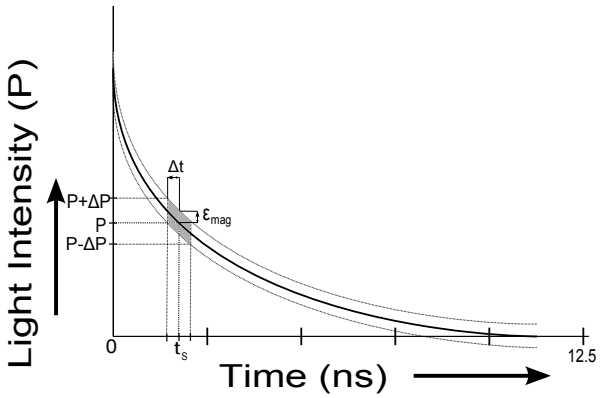

Figure D.5: Time-domain measurement with timing and magnitude errors included

The gray shaded area renders the measurement error area which is caused by the timing- and magnitude error. The figure indicates that a negative timing- and positive magnitude-error or vice versa yields a maximal error. The maximal τ-error that can occur results from an opposite maximal error for each time-sample. The conditions that yields a maximal τ-error are therefore described by:

$$\begin{aligned} \Delta t_1 &= -\Delta t \\ \varepsilon_{mag1} &= +\varepsilon_{mag} \\ \Delta t_2 &= +\Delta t \\ \varepsilon_{mag2} &= -\varepsilon_{mag} \end{aligned}$$

or

$$\begin{aligned} \Delta t_1 &= +\Delta t \\ \varepsilon_{mag1} &= -\varepsilon_{mag} \\ \Delta t_2 &= -\Delta t \\ \varepsilon_{mag2} &= +\varepsilon_{mag} \end{aligned}$$

where ε_{mag} and Δt are respectively the maximal magnitude-error and constant timing error that could occur.

Expression (D.1) yields τ for ideal measurement. Substituting the timing- and magnitude-errors described above in this expression yields:

$$\tau_\varepsilon = \frac{t_1 - t_2}{ln(\frac{f(t_2+\Delta t)-\varepsilon_m}{f(t_1-\Delta t)+\varepsilon_m})}$$

with

$$f(t+\Delta t) = F_0 \cdot e^{-\frac{t+\Delta t}{\tau}} \cdot \frac{1}{1-e^{-\frac{T}{\tau}}} = f(t) \cdot e^{-\frac{\Delta t}{\tau}}$$

this becomes:

$$\tau_\varepsilon = \frac{t_1 - t_2}{ln(\frac{f(t_2)\cdot e^{-\frac{\Delta t}{\tau}}-\varepsilon_m}{f(t_1)\cdot e^{\frac{\Delta t}{\tau}}+\varepsilon_m})} \tag{D.42}$$

The maximal magnitude error ε_{mag} can be obtained by subtracting τ from (D.42) and solving the result for this variable. This yields:

$$\begin{aligned}\varepsilon_{mag} &= \frac{f(t_2)\cdot e^{-\frac{\Delta t}{\tau}} - f(t_1)\cdot e^{\frac{t_1-t_2}{\tau+\varepsilon_\tau}} \cdot e^{\frac{\Delta t}{\tau}}}{1+e^{\frac{t_1-t_2}{\tau+\varepsilon_\tau}}} \\ &= \frac{F_0 \cdot \left(e^{-\frac{t_2+\Delta t}{\tau}} - e^{\frac{t_1-t_2}{\tau+\varepsilon_\tau}} \cdot e^{-\frac{t_1-\Delta t}{\tau}}\right)}{\left(1-e^{-\frac{T}{\tau}}\right)\cdot\left(1+e^{\frac{t_1-t_2}{\tau+\varepsilon_\tau}}\right)}\end{aligned} \tag{D.43}$$

The complete derivation of this expression is described in appendix (G.2.1).

The optimal values for the variables of the receiver can be acquired from the expressions derived above. Expression D.43 shows that the magnitude error dependents on multiple variables. Most factors are variables (F_0 and τ) and constants (T=1/80MHz) determined by the transmitter of the signal or other factors that are not compliant by the receiver (Δt). The only variables of the receiver are the sample times (t_1 and t_2). Because (D.43) contains multiple variables (t_1, t_2 and τ) the maximal allowed magnitude error for τ in the range of 1ns to 10ns can not be obtained by means of an algebraic analysis. However the influence of t_1 can be derived by observation from the expressions. The exponential functions with t_1 as power in the numerator of (D.43) cancel each other almost out because the factor ε_τ is very small compared to τ. Variable t_1 as power of the exponential function in the denominator is much larger and influences the behavior of the expression the most. To obtain a maximal value for ε_{mag}, the denominator of (D.43) should be as small as possible. Therefore t_1 should also be as small as possible; t_1=0 is taken. The relation between t_2 and ε_{max} is more difficult to derive and therefore the optimal value for t_2 is obtained by means of a numerical analysis. The value of Δt is also of influence on this result and since this value is obtained in section D.3, the optimal value for t_2 is also obtained in that section.

Extraction of τ: two area measurements

The extraction of τ by means of two area measurement also suffers from timing- and magnitude- measurement errors in practice. These errors are among other things introduced due to jitter, device noise, gain- and offset errors. As stated before, the maximal timing error is assumed fixed (Δt) and the device noise can be described by the maximal allowed magnitude error and is derived as function of t_1 and t_2 with constant Δt in this section.

The measurement errors are shown in figure D.6. The dark gray shaded area reflects the maximal possible negative area error introduced due to negative magnitude error and positive upper- and negative lower-integration limit errors. The light gray shaded area reflects the maximal possible positive area error introduced due to the contrary measurement errors. It can be concluded from the figure that a maximal τ-error appears if the first area measurement (integration from t_1 to t_2) suffers from a maximal positive area error and the second area measurement (integration from t_3 to t_4) suffers from a maximal negative area error, or vice versa. These situations are described by:

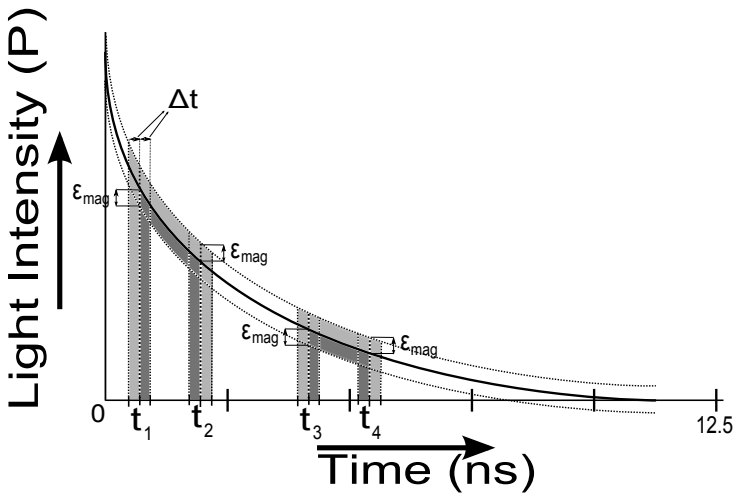

Figure D.6: Time-domain area measurement with timing errors and magnitude errors included

$$\begin{aligned} \Delta t_1 = -\Delta t_2 = -\Delta t_3 = \Delta t_4 = +\Delta t \\ \varepsilon_{area1} = -\varepsilon_{mag} \cdot (t_2 - t_1 - 2\Delta t) \\ \varepsilon_{area2} = +\varepsilon_{mag} \cdot (t_4 - t_3 + 2\Delta t) \end{aligned}$$

and

$$\begin{aligned} \Delta t_1 = -\Delta t_2 = -\Delta t_3 = \Delta t_4 = -\Delta t \\ \varepsilon_{area1} = +\varepsilon_{mag} \cdot (t_2 - t_1 + 2\Delta t) \\ \varepsilon_{area2} = -\varepsilon_{mag} \cdot (t_4 - t_3 - 2\Delta t) \end{aligned}$$

Substituting the measurement errors described for the first worst case situation in (D.20) which yields

$$\tau_\epsilon = -\frac{C_1}{ln\left(\frac{A(t_3-\Delta t,t_4+\Delta t)+\varepsilon_{mag}\cdot(t_4-t_3+2\Delta t)}{A(t_1+\Delta t,t_2-\Delta t)-\varepsilon_{mag}\cdot(t_2-t_1-2\Delta t)}\right)} \tag{D.44}$$

$$\tau_\epsilon = -\frac{C_2}{ln\left(\frac{A(t_3-\Delta t,t_4+\Delta t)+\varepsilon_{mag}\cdot(t_4-t_3+2\Delta t)}{A(t_1+\Delta t,t_2-\Delta t)-\varepsilon_{mag}\cdot(t_2-t_1-2\Delta t)}-1\right)} \tag{D.45}$$

Here C_1, C_2 and the conditions for $\{t_1, t_2, t_3, t_4\}$ are described by respectively (D.9-D.10) and (D.12-D.17). With $\tau_\epsilon = \tau + \epsilon_\tau$ and solving for ε_{mag} yields:

$$\varepsilon_{mag} = \frac{-F_0\cdot\tau}{1-e^{-\frac{T}{\tau}}}\cdot\frac{(e^{-\frac{t_2-\Delta t}{\tau}}-e^{-\frac{t_1+\Delta t}{\tau}})\cdot e^{-\frac{C_1}{\tau+\epsilon_\tau}}-(e^{-\frac{t_4+\Delta t}{\tau}}-e^{-\frac{t_3-\Delta t}{\tau}})}{t_4-t_3+2\cdot\Delta t+(t_2-t_1-2\cdot\Delta t)\cdot e^{-\frac{C_1}{\tau+\epsilon_\tau}}} \tag{D.46}$$

and

$$\varepsilon_{mag} = \frac{-F_0\cdot\tau}{1-e^{-\frac{T}{\tau}}}\cdot\frac{(e^{-\frac{t_2-\Delta t}{\tau}}-e^{-\frac{t_1+\Delta t}{\tau}})\cdot\left(e^{-\frac{C_2}{\tau+\epsilon_\tau}}+1\right)-(e^{-\frac{t_4+\Delta t}{\tau}}-e^{-\frac{t_3-\Delta t}{\tau}})}{t_4-t_3+2\cdot\Delta t+(t_2-t_1-2\cdot\Delta t)\cdot(e^{-\frac{C_2}{\tau+\epsilon_\tau}}+1)} \tag{D.47}$$

The steps to derive (D.46) and (D.47) from respectively (D.44) and (D.45) are described in appendix G.2.2.

These expressions show that the value of the maximal allowed magnitude error depends on multiple variables and constants from which only (t_1, t_2, t_3, t_4) are variables of the receiver. The optimal values for these variables have to be found for the worst situations that can occur. This worst case situation occurs for values of the variables determined by the transmitter that allow a minimal measurement error. Because multiple variables are of influence on the allowed measurement error, the optimal values for $\{t_1, t_2, t_3, t_4\}$ can not be obtained by means of an algebraic analysis. These values however can be obtained by numerical analysis. Because the value for Δt is determined in section D.3, this numerical analysis is also performed in that section. The numerical analysis yields however that the accuracy requirements are not feasible with the obtained timing error Δt.

Extraction of τ: two average area measurements

The extraction of τ by means of two average area measurements is a variant on the measurement of two areas method which is described in section D.1.1 and yield almost identical expressions for the extraction of τ. This also means that the expressions to determine the accuracy of the τ extraction will be almost identical to the expressions derived in D.2.1. Performing therefore the same derivation yields:

$$\tau_\epsilon = -\frac{C}{ln\left(\frac{AA(t_3-\Delta t,t_4+\Delta t)+\frac{\varepsilon_{area}}{t_4-t_3}}{AA(t_1+\Delta t,t_2-\Delta t)-\frac{\varepsilon_{area}}{t_2-t_1}} \cdot \frac{t_2-t_1}{t_4-t_3} - C_3\right)} \tag{D.48}$$

Where the area error ε_{area} is described by $\varepsilon_{mag} \cdot (t_2 - t_1)$. Substituting the conditions for $\{t_1, t_2, t_3, t_4, C, C_3\}$ which are described by respectively (D.9-D.10) and (D.12-D.17) in (D.48) yields respectively

$$\tau_\epsilon = -\frac{C}{ln\left(\frac{AA(t_3-\Delta t,t_4+\Delta t)+\varepsilon_{mag}}{AA(t_1+\Delta t,t_2-\Delta t)-\varepsilon_{mag}}\right)} \tag{D.49}$$

and

$$\tau_\epsilon = -\frac{C}{ln\left(2 \cdot \frac{AA(t_3-\Delta t,t_4+\Delta t)+\varepsilon_{mag}}{AA(t_1+\Delta t,t_2-\Delta t)-\varepsilon_{mag}} - 1\right)} \tag{D.50}$$

solving this for ε_{mag} yields

$$\varepsilon_{mag} = \frac{-F_0 \cdot \tau}{1 - e^{-\frac{T}{\tau}}} \cdot \frac{\frac{e^{-\frac{t_2-\Delta t}{\tau}} - e^{-\frac{t_1+\Delta t}{\tau}}}{(t_2-t_1-2\cdot\Delta t)} \cdot e^{-\frac{C_1}{\tau+\epsilon_\tau}} - \frac{e^{-\frac{t_4+\Delta t}{\tau}} - e^{-\frac{t_3-\Delta t}{\tau}}}{t_4-t_3+2\cdot\Delta t}}{e^{-\frac{C_1}{\tau+\epsilon_\tau}} + 1} \tag{D.51}$$

and

$$\varepsilon_{mag} = \frac{-F_0 \cdot \tau}{1 - e^{-\frac{T}{\tau}}} \cdot \frac{\frac{e^{-\frac{t_2-\Delta t}{\tau}} - e^{-\frac{t_1+\Delta t}{\tau}}}{t_2-t_1-2\cdot\Delta t} \cdot \left(e^{-\frac{C_2}{\tau+\epsilon_\tau}} + 1\right) - 2 \cdot \frac{e^{-\frac{t_4+\Delta t}{\tau}} - e^{-\frac{t_3-\Delta t}{\tau}}}{t_4-t_3+2\cdot\Delta t}}{e^{-\frac{C_2}{\tau+\epsilon_\tau}} + 3} \tag{D.52}$$

These expressions again show that a numerical analysis is necessary to obtain the optimal variable values, the maximal allowed magnitude error (ε_{mag}) that has to be achieved. This is also performed in section D.3.

D.2.2 Frequency-domain methods to extract τ

Extraction of τ: measurement of two frequency-components

The measurement of two frequency samples can be affected by magnitude errors, phase errors and frequency-mixing errors (e.g. mixing with 79.9MHz instead of 80MHz). The latter error does not affect the τ extraction accuracy in a direct way (e.g. the magnitude is not affected). It is already described that the complex frequency components consists of a real and imaginary part. Measuring the magnitude of the complex signal requirers mixing of the each individual part. This is called quadrature mixing. The real part is mixed by a cosine and the imaginary part by a sine. This is already described in section D.1.2 and D.1.2. It is also described further on in section D.2.2 that a phase error results also mixing of of the 'wrong' part of the complex component. This is described by expression D.59 where a_n corresponds to the real and b_n to the complex part of the signal. The phase error is in essence a time error described in another domain. It is described that a constant value is taken for the timing error and thus also the phase error such that the measurement can be optimized with respect to a maximal allowed magnitude error. Therefore the influence of the magnitude error is first elaborated. The influence of this error on the τ extraction is described by

$$\tau_\epsilon = \sqrt{\frac{\left(\frac{|K(\omega_2)|+\varepsilon_2}{|K(\omega_1)|+\varepsilon_1}\right)^2 - 1}{\omega_1^2 - \left(\frac{|K(\omega_2)|+\varepsilon_2}{|K(\omega_1)|+\varepsilon_1}\right)^2 \cdot \omega_2^2}} \tag{D.53}$$

where ε_1 and ε_2 are the magnitude errors of respectively the first and second independent frequency component that is measured. The worst case situation occurs with $\varepsilon_1 = -\varepsilon_2 = \pm\varepsilon_{max}$. Subtracting τ from (D.53) results in the absolute τ-error (ϵ_τ). Replacing the magnitude errors by the worst case errors and solving this for ε_{mag} yields:

$$\varepsilon_{max} = \frac{|K(\omega_2)| - |K(\omega_1)| \cdot \sqrt{\frac{1+\omega_1^2\cdot(\epsilon_\tau+\tau)^2}{1+\omega_2^2\cdot(\epsilon_\tau+\tau)^2}}}{1 + \sqrt{\frac{1+\omega_1^2\cdot(\epsilon_\tau+\tau)^2}{1+\omega_2^2\cdot(\epsilon_\tau+\tau)^2}}} \tag{D.54}$$

The entire derivation is described in G.2.4.

The derivations for the measurement of only a real or only a complex part of the frequency components can be elaborated at exactly the same way. This is yields

$$\varepsilon_{max} = -\frac{K_I(\omega_2) - K_I(\omega_1) - (\tau+\varepsilon_\tau)^2 \left(\omega_1^2 K_I(\omega_1) - \omega_2^2 K_I(\omega_2)\right)}{(\tau+\varepsilon_\tau)^2 (\omega_1^2 - \omega_2^2) + 2} \tag{D.55}$$

for the real component measurement. In section D.3 it is obtained that measuring the DC component is essential for an accurate measurement for the whole

complex signal and the real part of the signal. The complex function however does not embrace a component at DC and is therefore not appropriate.

The feasible accuracy of the measurement of these individual parts and the whole complex signal is described in chapter D.3.

Extraction of τ: I and Q frequency measurement

Magnitude and phase errors could occur while performing an I and Q measurement. The influence of magnitude errors are described by the next expressions:

$$a_n^* = a_n + \varepsilon_{magA}$$
$$b_n^* = b_n + \varepsilon_{magB}$$

Phase errors occur while performing an I and Q demodulation. These phase errors ,ϕ_I and ϕ_Q , yields multiplication of (D.1.2) with respectively $\cos(n\omega_0 t + \phi_I)$ and $\sin(n\omega_0 t + \phi_Q)$ described by respectively

$$f_{I+\varepsilon}(t) = a_n \cos(n\omega_0 t)\cos(n\omega_0 t + \phi_I) + b_n \sin(n\omega_0 t)\cos(n\omega_0 t + \phi_I)$$

and

$$f_{Q+\varepsilon}(t) = a_n \cos(n\omega_0 t)\sin(n\omega_0 t + \phi_Q) + b_n \sin(n\omega_0 t)\sin(n\omega_0 t + \phi_Q)$$

Using standard trigonometric identities, which are described in appendix (E.12), with phase error included, the expressions can be written as respectively

$$\begin{aligned} f_{I+\varepsilon}(t) &= \frac{1}{2}a_n[\cos(\phi_I) + \cos(2\omega_0 t + \phi_I)] + \frac{1}{2}b_n[\sin(\phi_I) + \sin(2\omega_0 t + \phi_I)] \\ &= \frac{1}{2}a_n\cos(\phi_I) + \frac{1}{2}b_n\sin(\phi_I) + \frac{1}{2}[a_n\cos(2\omega_0 t + \phi_I) + b_n\sin(2\omega_0 t + \phi_I)] \end{aligned} \tag{D.56}$$

and

$$f_{Q+\varepsilon}(t) = \frac{1}{2}b_n\cos(\phi_Q) + \frac{1}{2}a_n\sin(\phi_Q) + \frac{1}{2}[a_n\sin(2\omega_0 t + \phi_Q) - b_n\cos(2\omega_0 t + \phi_Q)] \tag{D.57}$$

low-pass filtering yields:

$$f_{I+\varepsilon}(t) = \frac{1}{2}a_n\cos(\phi_I) + \frac{1}{2}b_n\sin(\phi_I) \tag{D.58}$$
$$f_{Q+\varepsilon}(t) = \frac{1}{2}b_n\cos(\phi_Q) + \frac{1}{2}a_n\sin(\phi_Q) \tag{D.59}$$

Substituting the magnitude errors in (D.59) yields an expression that describes the function with both measurement errors included:

$$f_{I+\varepsilon}(t) = \frac{1}{2}(a_n + \varepsilon_a)\cos(\phi_I) + \frac{1}{2}(b_n + \varepsilon_b)\sin(\phi_I) \tag{D.60}$$

$$f_{Q+\varepsilon}(t) = \frac{1}{2}(b_n + \varepsilon_b)\cos(\phi_Q) + \frac{1}{2}(a_n + \varepsilon_a)\sin(\phi_Q) \tag{D.61}$$

In the ideal case (no measurement errors) only $\frac{1}{2}a_n$ and $\frac{1}{2}b_n$ remain for respectively $f_I(t)$ and $f_Q(t)$. So in the practical case multiple error factors are added to the ideal signal. The worst case situation occurs if the error of one part is maximal positive and the error of the other is maximal negative or vice versa. Expression (D.60) and (D.61) indicate that this occurs if the sign of ε_a and ϕ_I is the same and opposite to the sign of ε_b and ϕ_Q ,which is also the same. So the worst case situations are described by

$$\begin{aligned}\varepsilon_a &= \varepsilon_{mag}\\ \varepsilon_b &= -\varepsilon_{mag}\\ \phi_I &= \phi_{max}\\ \phi_Q &= -\phi_{max}\end{aligned}$$

and

$$\begin{aligned}\varepsilon_a &= -\varepsilon_{mag}\\ \varepsilon_b &= \varepsilon_{mag}\\ \phi_I &= -\phi_{max}\\ \phi_Q &= \phi_{max}\end{aligned}$$

Expressions (D.36) and (D.37) describe the functions in the ideal case. However because an error is incorporated in $f_{I+\varepsilon}(t)$ and $f_{Q+\varepsilon}(t)$ these functions are described by

$$f_{I+\varepsilon}(t) = \frac{F_S F_0 \tau_\varepsilon}{1 + (n\omega_0\tau_\varepsilon)^2} \tag{D.62}$$

$$f_{Q+\varepsilon}(t) = \frac{F_S F_0 \tau_\varepsilon^2 n\omega_0}{1 + (n\omega_0\tau_\varepsilon)^2} \tag{D.63}$$

with $\tau_\varepsilon = \tau + \varepsilon_\tau$

Substituting (D.62),(D.63) and the first described worst case situation in (D.59) yields

$$\frac{1}{2}(a_n + \varepsilon_{mag})\cos(\phi_{max}) + \frac{1}{2}(b_n - \varepsilon_{mag})\sin(\phi_{max}) = \frac{F_S F_0 \tau_\varepsilon}{1 + (n\omega_0\tau_\varepsilon)^2} \tag{D.64}$$

$$\frac{1}{2}(b_n - \varepsilon_{mag})\cos(-\phi_{max}) + \frac{1}{2}(a_n + \varepsilon_{mag})\sin(-\phi_{max}) = \frac{F_S F_0 \tau_\varepsilon^2 n\omega_0}{1 + (n\omega_0\tau_\varepsilon)^2} \tag{D.65}$$

Combining the expressions and solving this for ε_{mag} yields

$$\varepsilon_{mag} = \frac{-\varepsilon_\tau n\omega_0\cos(\phi_{max}) - (\varepsilon_\tau + \tau)\cdot\tau n^2\omega_0^2\sin(\phi_{max}) - \sin(\phi_{max})}{(\varepsilon_\tau + \tau)\cdot n\omega_0\left(\cos(\phi_{max}) - \sin(\phi_{max})\right) + \sin(\phi_{max}) + \cos(\phi_{max})} \cdot \frac{2F_S F_0 \tau}{1 + (n\omega_0\tau)^2} \tag{D.66}$$

The steps to derive (D.66) out of (D.65) are described in appendix G.2.4.

For this measurement error, n is the only variable of the receiver. To acquire the maximal allowed magnitude error for this method the optimal value for n has to be obtained. Expression (D.66) contains n^2 multiplied with the largest weight in the denominator of the function and therefore a minimal value for n yields a maximal allowed magnitude error. Because the independent frequency component at 0Hz does not contain an imaginary part, the value 1 is taken for n. Also the worst case value for τ, in the range from 1ns to 10ns, has to be found. This is then the value that yields minimal allowed magnitude error. The expression contains τ^2 multiplied with the largest weight in the denominator and therefore the maximal value (10ns) describes the worst case situation.

The value of ϕ_{max} is required to derive the maximal allowed magnitude error. This value is however determined in section D.3 and therefore ε_{mag} and SNR are also derived in that section. This derivation yields that that the accuracy requirements are not feasible with the obtained timing error Δt.

D.3 Comparison of the described methods

To determine the fixed value for the timing errors, it has to be determined what the origin of the errors is. Timing errors are mainly caused by clock generation errors and clock generators are commonly implemented as a phase-locked loop (PLL). Therefore the timing accuracy of a PLL has to be discovered. A literature investigation is performed to find out which figures are feasible. To find representative figures, the requirements of the concerned publications and this research like implemented technology, supply range and frequency range should correspond. Analysis of [11] shows that minimal jitter that can be acquired with a PLL is independent of the output frequency for a given power budget. Therefore the implemented technology and supply range are the only requirements that should correspond. The technology used for this research, ABCD9 CMOS 140nm, shows great resemblance with the 130nm CMOS process. Therefore PLL circuits implemented in CMOS 130nm are analyzed. To obtain the worst case errors, the maximal timing error should be obtained and therefore the peak-to-peak jitter has to be determined. In [12] it is presented how the RMS jitter , which is mainly presented in PLL publications, is converted to peak-to-peak jitter at a specified bit error rate (BER). The results of the literature research is given in table D.1 where the most right row presents the peak-to-peak jitter.

Ref.	technology	Jitter (rms)	Jitter(p-p)
[13]	130	0.5	3.29
[14]	130	0.64	4.21
[15]	130	-	18.55
[16]	130	1.0	6.58

Table D.1: Jitter specifications of PLL designs

The represented publications describe high performance designs and therefore a value of 5ps peak-to-peak jitter is assumed for the comparison of the various methods described in section D.1.

The methods are compared with respect to the maximal allowed magnitude errors, with constant $F_0 = 0.01$, and minimal needed SNR. The SNR of all functions is equal to F_0 divided by the allowed magnitude errors.

Extraction of τ: measurement of two time-samples

The goal of this section is to optimize the allowed magnitude error and obtain the corresponding values. Values for the variables of the receiver (t_1 and t_2) have to be derived that allow an as high as possible magnitude error that still meets the accuracy of the extraction of τ. This is accomplished when the optimal values for t_1 and t_2 are derived for (D.43). This expression is described by

$$\varepsilon_{mag} = \frac{F_0 \cdot \left(e^{-\frac{t_2+\Delta t}{\tau}} - e^{\frac{t_1-t_2}{\tau+\varepsilon_\tau}} \cdot e^{-\frac{t_1-\Delta t}{\tau}} \right)}{\left(1 - e^{-\frac{T}{\tau}}\right) \cdot \left(1 + e^{\frac{t_1-t_2}{\tau+\varepsilon_\tau}}\right)}$$

The maximal timing error (Δt) and the maximal allowed τ-error (ε_τ) are constants and are respectively 10ps and 49ps. In section D.2 it is already noticed that a minimal value for t_1 yields a maximal magnitude error and therefore this value is set to 0ns. A numerical analysis is performed to obtain the optimal value for t_2.

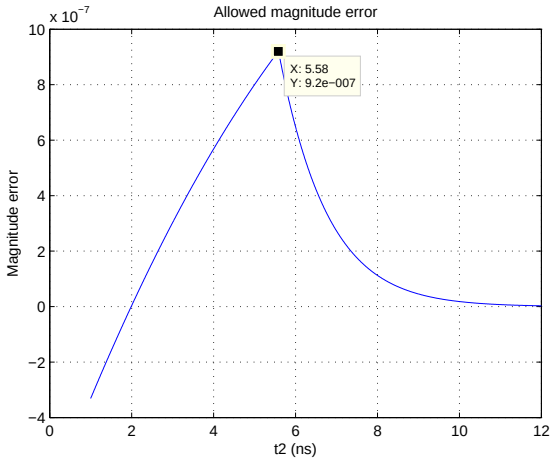

Figure D.7: Magnitude error measurement

Figure D.7 presents the results of this numerical analysis with F_0=1m and shows that a maximal magnitude error is acquired around t_2=5.58ns. With t_1=0, the maximal allowed magnitude error becomes 0.92μ. This corresponds with an SNR of 1080 or 60.7 dB.

Extraction of τ: two area measurements

This method can be divided into two situations. For the first situation the integration limits $\{t_1, t_2, t_3, t_4\}$ have to meet the restrictions described by (D.9-D.10) and for the second situation the restrictions described by (D.12-D.17) have to be met. The minimal SNR that have to be reached to meet the specified τ extraction accuracy (100ps) is described by respectively (D.46) and (D.47) which are reflected by

$$\varepsilon_{mag} = \frac{-F_0 \cdot \tau}{1 - e^{-\frac{T}{\tau}}} \cdot \frac{(e^{-\frac{t_2 - \Delta t}{\tau}} - e^{-\frac{t_1 + \Delta t}{\tau}}) \cdot e^{-\frac{C_1}{\tau + \epsilon_\tau}} - (e^{-\frac{t_4 + \Delta t}{\tau}} - e^{-\frac{t_3 - \Delta t}{\tau}})}{t_4 - t_3 + 2 \cdot \Delta t + (t_2 - t_1 - 2 \cdot \Delta t) \cdot e^{-\frac{C_1}{\tau + \epsilon_\tau}}}$$

and

$$\varepsilon_{mag} = \frac{-F_0 \cdot \tau}{1 - e^{-\frac{T}{\tau}}} \cdot \frac{(e^{-\frac{t_2 - \Delta t}{\tau}} - e^{-\frac{t_1 + \Delta t}{\tau}}) \cdot \left(e^{-\frac{C_2}{\tau + \epsilon_\tau}} + 1\right) - (e^{-\frac{t_4 + \Delta t}{\tau}} - e^{-\frac{t_3 - \Delta t}{\tau}})}{t_4 - t_3 + 2 \cdot \Delta t + (t_2 - t_1 - 2 \cdot \Delta t) \cdot (e^{-\frac{C_2}{\tau + \epsilon_\tau}} + 1)}$$

To acquire the minimal allowed SNR that can be reached first the optimal values for $\{t_1, t_2, t_3, t_4\}$ have to be obtained by performing a numerical analysis.

First the first situation is analyzed. Expressions (D.46) holds several variables, namely t_1, t_2, t_3, t_4, C_1 and τ. Because each variable increases the possible combinations exponentially, this numerical analysis embraces many combinations. The restrictions for the integration limits and C_1 described by (D.9-D.10) show a relation between the variables and therefore the number of variables can be decreased. The variables can be written as:

$$\begin{aligned} t_2 &= t_1 + t_\Delta \\ t_3 &= t_1 + C_1 \\ t_4 &= t_1 + C_1 + t_\Delta \end{aligned}$$

This shows that the number of variables is decreased with 2. It can be derived that the variable t_1 is only present in the power of the exponential function in the denominator of the expression. To acquire an as large as possible magnitude error, this factor has to be as big as possible and therefore t_1 has to be as small as possible. Therefore this value is set to 0ns. A numerical analysis is performed to find the optimal values for t_Δ and C_1

Figure D.8 presents the results of this numerical analysis with F_0=1m and shows that all allowed magnitude errors are negative. This means that the τ accuracy of 49ps can not be achieved with the specified timing error of 5ps.

For the second situation the expression can also be simplified. The variable t_1 is only present in the power of the exponential function in the denominator of

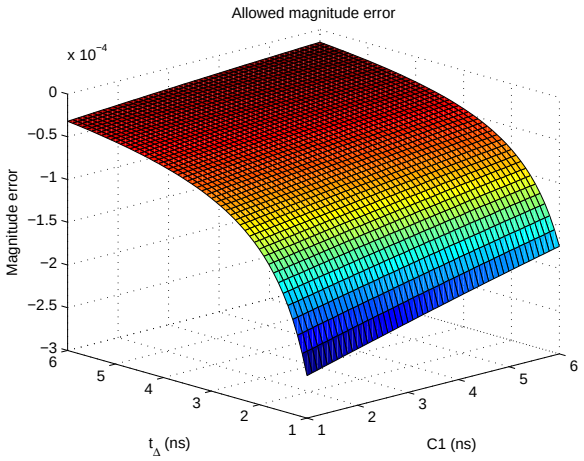

Figure D.8: Magnitude error measurement situation 1

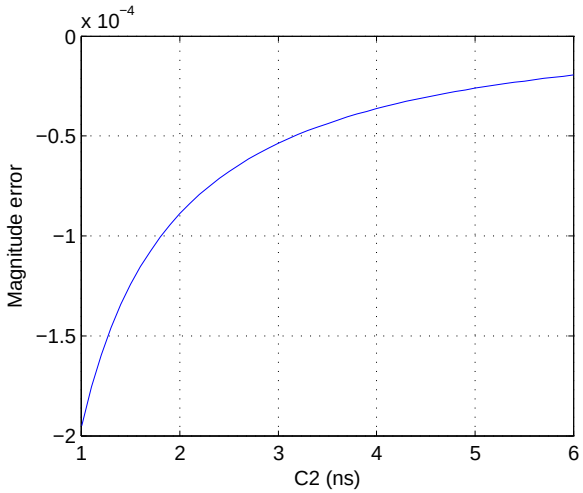

Figure D.9: Magnitude error measurement situation 2

the expression and therefore the value 0ns yields a maximal allowed error. The optimal value for C_2 again can be acquired with a numerical analysis.

Figure D.9 presents the results of this numerical analysis with F_0=1m and shows that again all allowed magnitude errors are negative. This also means that this situation can not meet the accuracy constraint of 49ps.

Extraction of τ: two average area measurements

The accuracy expressions of two average area measurement, described by (D.46) for situation one and (D.47) for situation two, are very similar to the accuracy expressions of two area measurement and therefore the same steps are performed as described in D.3.

$$\varepsilon_{mag} = \frac{-F_0 \cdot \tau}{1 - e^{-\frac{T}{\tau}}} \cdot \frac{(e^{-\frac{t_2-\Delta t}{\tau}} - e^{-\frac{t_1+\Delta t}{\tau}}) \cdot e^{-\frac{C_1}{\tau+\epsilon_\tau}} - (e^{-\frac{t_4+\Delta t}{\tau}} - e^{-\frac{t_3-\Delta t}{\tau}})}{t_4 - t_3 + 2 \cdot \Delta t + (t_2 - t_1 - 2 \cdot \Delta t) \cdot e^{-\frac{C_1}{\tau+\epsilon_\tau}}}$$

and

$$\varepsilon_{mag} = \frac{-F_0 \cdot \tau}{1 - e^{-\frac{T}{\tau}}} \cdot \frac{(e^{-\frac{t_2-\Delta t}{\tau}} - e^{-\frac{t_1+\Delta t}{\tau}}) \cdot \left(e^{-\frac{C_2}{\tau+\epsilon_\tau}} + 1\right) - (e^{-\frac{t_4+\Delta t}{\tau}} - e^{-\frac{t_3-\Delta t}{\tau}})}{t_4 - t_3 + 2 \cdot \Delta t + (t_2 - t_1 - 2 \cdot \Delta t) \cdot (e^{-\frac{C_2}{\tau+\epsilon_\tau}} + 1)}$$

A numerical analysis is performed to find the optimal values for t_1, t_Δ and C_1 and C_2. With t_1=0 maximal accuracy is obtained. The numerical analysis for situation 2 yields negative values and is therefore not feasible.

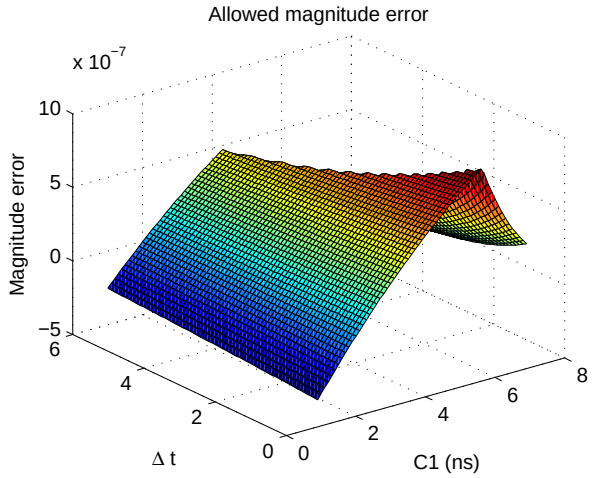

Figure D.10: Magnitude error measurement situation 1

Figure D.10 and D.11 present the results of the numerical analysis with F_0=1m for situation 1, where the values of $\{t_1, t_2, t_3, t_4\}$ described by (D.9-D.10). The maximal allowed magnitude error ε_{mag} equals 0.93 μ which corresponds with an SNR of 1000 or 60dB. These values are however obtained with $t_2 - t_1 = 0.1ns$ which is practical hard to perform. Therefore the numerical analysis is also performed with $t_2 - t_1 = 1ns$. This yields; ε_{mag}=0.81μ which corresponds with an SNR of 1234 or 61.8dB.

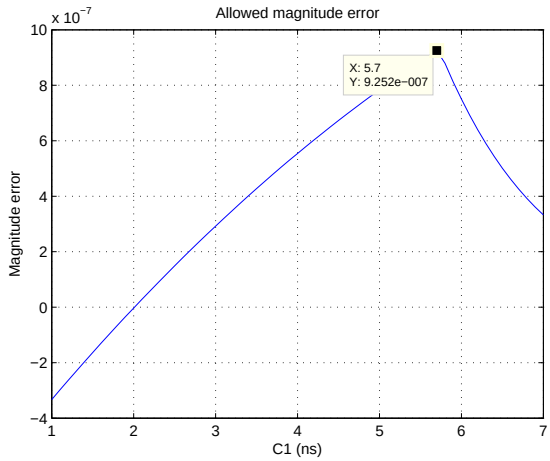

Figure D.11: Magnitude error measurement situation 1

Extraction of τ: measurement of two frequency components

To obtain the optimal values for ω_1 and ω_2 a numerical analysis is performed for τ=1-10ns and for different combinations of ω_1 and ω_2. The phase error for the worst case situation is included as a constant. The factor F_0 shows a linear relation with ε_{mag} and is therefore taken constant (1m) in the analysis. The results of the analysis are shown in table D.2, showing that a value of 0Hz and $2\pi\cdot$160MHz for respectively ω_1 and ω_2 yield a maximal value for ϵ_{mag} (3.1945μ). The combination of the components with $n_1 \neq 0$ yield a negative allowed magnitude which implies that the required accuracy is not feasible with the included phase error. To compare the methods, the minimal allowed SNR also has to be obtained. The SNR equals the ratio between the maximum magnitude and F_0 and yields 3130 or 69.9dB with optimal values.

ω_1	ω_2	$\epsilon_{mag}(\cdot 10^{-7})$	SNR
0	1	3.0954	$3.23 \cdot 10^3$
0	2	3.1945	$3.13 \cdot 10^3$
0	3	2.2953	$4.36 \cdot 10^3$
0	4	1.7849	$5.60 \cdot 10^3$

Table D.2: List with maximal permitted magnitude error for different combinations of ω_1 and ω_2.

A numerical analysis is also performed for the measurement of the real parts of the individual components. This however results a negative allowed magnitude error which also implies that the required accuracy is not feasible with the included phase error.

Extraction of τ: I and Q frequency measurement

The maximal allowed magnitude error have to be obtained in this section. These values can be derived with expression D.66. The independent frequency component that yields maximal allowed measurement errors is already obtained in section D.2 and is situated at $n \cdot \omega_0 = \omega_0$; n=1 . The worst case situation is also determined in this section and occurs for τ=10ns. Therefore only the phase error has to be obtained to derive the maximal allowed magnitude error and the minimal allowed SNR.

A phase error can also be described as a timing error and therefore ϕ_{max} can be derived from the value obtained at the start of this section. A phase error can be described in radians by the ratio between the timing error and the period time multiplied with 2π. With quadrature demodulation the received signal is mixed with respectively $\cos(n\omega_0)$ and $\sin(n\omega_0)$. With n=1, the period time is equal to the period time of the received signal (12.5ns). The phase error therefore becomes: $\frac{10ps}{12.5ns} \cdot 2\pi = 5.0 \cdot 10^{-3}$.

Substituting the derived values with F_0=1m in (D.66) yields a negative value for ε_{mag}. This means that this method can not meet the accuracy constraints of 49ps.

Appendix E

Standard formulas

E.1 Trigonometric identities

The product-to-sum identities can be described by

$$\cos(\theta)\cos(\beta) = \frac{\cos(\theta-\beta)+\cos(\theta+\beta)}{2} \tag{E.1}$$

$$\sin(\theta)\sin(\beta) = \frac{\cos(\theta-\beta)-\cos(\theta+\beta)}{2} \tag{E.2}$$

$$\sin(\theta)\cos(\beta) = \frac{\sin(\theta-\beta)+\sin(\theta+\beta)}{2} \tag{E.3}$$

$$\tag{E.4}$$

With $\theta = \beta$ this becomes

$$\cos(\theta)\cos(\theta) = \frac{1+\cos(2\theta)}{2} \tag{E.5}$$

$$\sin(\theta)\sin(\theta) = \frac{1-\cos(2\theta)}{2} \tag{E.6}$$

$$\sin(\theta)\cos(\theta) = \frac{0+\sin(2\theta)}{2} \tag{E.7}$$

$$\tag{E.8}$$

Inserting a phase error ϕ yields

$$\cos(\theta)\cos(\theta+\phi) = \frac{\cos(-\phi)+\cos(2\theta)}{2} \tag{E.9}$$

$$\sin(\theta)\sin(\theta+\phi) = \frac{\cos(-\phi)-\cos(2\theta)}{2} \tag{E.10}$$

$$\sin(\theta)\cos(\theta+\phi) = \frac{\sin(-\phi)+\sin(2\theta)}{2} \tag{E.11}$$

$$\tag{E.12}$$

Appendix F

Non-linearity analysis

A property of active circuits is that the input to output transfer has a non-linear relation. The input to output characteristic of a non-linear system can be described by the Taylor approximation [5]:

$$y(t) = \alpha_1 x(t) + \alpha_2 x^2 t + \alpha_3 x^3 t + ... \tag{F.1}$$

Where $\alpha_2 x^2 t$ and $\alpha_3 x^3 t$ describe respectively the second order and third order linearity components of the system. Figure 5.5 shows that the spectrum of the received signal is very broad and contains an independent frequency component at each integer multiple of the fundamental frequency F_S (80MHz). In section D.1.2 it is described that each component is described by $a_n \cos(n\omega_0 t) + ib_n \sin(n\omega_0 t)$ where a_n and b_n are described by respectively (D.34) and (D.35). The influence of intermodulation due to second order non-linearity between the components can be obtained by substituting the real parts of two random independent frequency components in the second order non-linearity product of (F.1):

$$\begin{aligned} y_2(t) &= \alpha_2 \cdot \Big(a_{n_1} \cos(n_1\omega_0 t) + a_{n_2} \cos(n_2\omega_0 t)\Big)^2 \\ &= \alpha_2 \cdot \Big(a_{n_1}^2 \cos(n_1\omega_0 t)^2 + a_{n_2}^2 \cos(n_2\omega_0 t)^2 + a_{n_1} \cos(n_1\omega_0 t) \cdot a_{n_2} \cos(n_2\omega_0 t)\Big) \\ &= \frac{\alpha_2}{2}\Big(a_{n_1}^2[1 + \cos(2n_1\omega_0 t)] + a_{n_2}^2[1 + \cos(2n_2\omega_0 t)] \\ &\quad + a_{n_2}a_{n_1}[\cos((n_1 + n_2)\omega_0 t) + \cos((n_1 - n_2)\omega_0 t)]\Big) \end{aligned} \tag{F.2}$$

Expression (F.2) shows that multiple frequency components originate from the second order non-linearity at integer multiples of ω_0 with a magnitude of respectively $\frac{\alpha_2}{2}a_{n_1}^2$, $\frac{\alpha_2}{2}a_{n_2}^2$ and $\frac{\alpha_2}{2}a_{n_1}a_{n_1}$.

A sinusoid can be applied as input signal to obtain the non-linearity coefficients

α_j . If $x(t) = A\cos(\omega\, t)$ is substituted in F.1 then the next output results:

$$y(t) = \frac{\alpha_2 A^2}{2} + \left(\alpha_1 A + \frac{3\alpha_3 A^3}{4}\right)\cos(\omega t) + \frac{\alpha_2 A^2}{2}\cos(2\omega t) + \frac{\alpha_3 A^3}{4}\cos(3\omega t) \tag{F.3}$$

The non-linearity coefficients subsequently can be obtained by simulating the magnitude of the second and third order harmonic.

Appendix G

Derivations for system design methods

G.1 System design methods

G.1.1 Extraction of τ: I and Q frequency measurement

$$a_n = \frac{2}{T}\int_0^T f(t)\cos(n\omega_0 t)\,dt \tag{G.1}$$

substituting (C.2) in (G.1) with $\frac{1}{T} = F_S$ yields

$$a_n = \frac{2F_S F_0}{1-e^{-\frac{T}{\tau}}}\int_0^T e^{-\frac{t}{\tau}}\cos(n\omega_0 t)\,dt \tag{G.2}$$

Integration by parts [17] is used to solve the integral. The next standard forms [17] can be used:

$$\int e^{at}\cos(bt)dt = \frac{e^{at}}{a^2+b^2}\left(a\cos(bt)+b\sin(bt)\right) \tag{G.3}$$

Substitute 'a' by $1/\tau$ and 'b' with $n\omega_0$ and substituting the result in (G.1.1) yields:

$$a_n = \frac{2F_S F_0}{1-e^{-\frac{T}{\tau}}}\left[\frac{e^{-\frac{t}{\tau}}}{(\frac{1}{\tau})^2+(n\omega_0)^2}\left(-\frac{1}{\tau})\cos(n\omega_0 t)+n\omega_0\sin(n\omega_0 t)\right)\right]_0^T \tag{G.4}$$

with $T = \frac{2\pi}{\omega_0}$ this yields

$$a_n = \frac{2F_S F_0}{1-e^{-\frac{T}{\tau}}}\frac{-\frac{1}{\tau}(e^{-\frac{T}{\tau}}-1)}{\frac{1}{\tau^2}+(n\omega_0)^2} \tag{G.5}$$

$$= \frac{2F_S F_0\tau}{1+(n\omega_0\tau)^2} \tag{G.6}$$

With the standard integral for $e^{at}\cos(bt)$ described by

$$\int e^{at}\sin(bt)dt = \frac{e^{at}}{a^2+b^2}\left(a\sin(bt) - b\cos(bt)\right) \tag{G.7}$$

the expression for b_n can be derived performing the same steps. This yields

$$a_n = \frac{2F_S F_0}{1-e^{-\frac{T}{\tau}}}\left[\frac{e^{-\frac{t}{\tau}}}{(\frac{1}{\tau})^2+(n\omega_0)^2}\left(-\frac{1}{\tau})\sin(n\omega_0 t) - n\omega_0\cos(n\omega_0 t)\right)\right]_0^T \tag{G.8}$$

$$= \frac{2F_S F_0 \tau^2 n\omega_0}{1+(n\omega_0\tau)^2} \tag{G.9}$$

G.2 Accuracy of the system design methods

G.2.1 Extraction of τ: measurement of two time samples

Substituting $\varepsilon_1 = -\varepsilon_2 = \pm\varepsilon_{max}$ in (D.42), subtract τ and solve the result for ε_{max} yields the next derivation:

$$\varepsilon_\tau = \frac{t_1 - t_2}{ln\left(\frac{f(t_2)\cdot e^{\frac{-\Delta t}{\tau}} - \varepsilon_{max}}{f(t_1)\cdot e^{\frac{\Delta t}{\tau}} + \varepsilon_{max}}\right)} - \tau \tag{G.10}$$

$$\frac{f(t_2)\cdot e^{\frac{-\Delta t}{\tau}} - \varepsilon_{max}}{f(t_1)\cdot e^{\frac{\Delta t}{\tau}} + \varepsilon_{max}} = e^{\frac{t_1-t_2}{\varepsilon_\tau+\tau}} \tag{G.11}$$

$$\varepsilon_{max}\cdot\left(1+e^{\frac{t_1-t_2}{\varepsilon_\tau+\tau}}\right) = f(t_2)\cdot e^{\frac{-\Delta t}{\tau}} - e^{\frac{t_1-t_2}{\varepsilon_\tau+\tau}}\cdot f(t_1)\cdot e^{\frac{\Delta t}{\tau}} \tag{G.12}$$

$$\varepsilon_{max} = \frac{f(t_2)\cdot e^{\frac{-\Delta t}{\tau}} - e^{\frac{t_1-t_2}{\varepsilon_\tau+\tau}}\cdot f(t_1)\cdot e^{\frac{\Delta t}{\tau}}}{1+e^{\frac{t_1-t_2}{\varepsilon_\tau+\tau}}} \tag{G.13}$$

Substituting (C.2) in (G.13) yields:

$$\varepsilon_{max} = \frac{F_0\cdot\left(e^{-\frac{t_2+\Delta t}{\tau}} - e^{\frac{t_1-t_2}{\tau+\varepsilon_\tau}}\cdot e^{-\frac{t_1-\Delta t}{\tau}}\right)}{\left(1-e^{-\frac{T}{\tau}}\right)\cdot\left(1+e^{\frac{t_1-t_2}{\tau+\varepsilon_\tau}}\right)} \tag{G.14}$$

G.2.2 Extraction of τ: two area measurements

$$\tau_\epsilon = -\frac{C_1}{ln\left(\frac{A(t_3-\Delta t,t_4+\Delta t)+\varepsilon_{mag}\cdot(t_4-t_3+2\Delta t)}{A(t_1+\Delta t,t_2-\Delta t)-\varepsilon_{mag}\cdot(t_2-t_1-2\Delta t)}\right)} \tag{G.15}$$

$$\tau_\epsilon = -\frac{C_2}{ln\left(\frac{A(t_3-\Delta t,t_4+\Delta t)+\varepsilon_{mag}\cdot(t_4-t_3+2\Delta t)}{A(t_1+\Delta t,t_2-\Delta t)-\varepsilon_{mag}\cdot(t_2-t_1-2\Delta t)}-1\right)} \tag{G.16}$$

The next steps are performed to solve (G.15) for ε_{mag} with $\tau_\epsilon = \tau + \epsilon_\tau$

$$\frac{A(t_3-\Delta t,t_4+\Delta t)+\varepsilon_{mag}\cdot(t_4-t_3+2\Delta t)}{A(t_1+\Delta t,t_2-\Delta t)-\varepsilon_{mag}\cdot(t_2-t_1-2\Delta t)} = e^{-\frac{C_1}{\tau+\epsilon_\tau}} \tag{G.17}$$

$$A(t_3-\Delta t,t_4+\Delta t)+\varepsilon_{mag}\cdot(t_4-t_3+2\Delta t) = e^{-\frac{C_1}{\tau+\epsilon_\tau}}\cdot(A(t_1+\Delta t,t_2-\Delta t)-\varepsilon_{mag}\cdot(t_2-t_1-2\Delta t)) \tag{G.18}$$

$$\varepsilon_{mag}\cdot(t_4-t_3+2\Delta t+e^{-\frac{C_1}{\tau+\epsilon_\tau}}\cdot(t_2-t_1-2\Delta t)) = e^{-\frac{C_1}{\tau+\epsilon_\tau}}\cdot A(t_1+\Delta t,t_2-\Delta t)-A(t_3-\Delta t,t_4+\Delta t) \tag{G.19}$$

$$\varepsilon_{mag} = \frac{A(t_1+\Delta t,t_2-\Delta t)\cdot e^{-\frac{C_1}{\tau+\epsilon_\tau}}-A(t_3-\Delta t,t_4+\Delta t)}{t_4-t_3+2\cdot\Delta t+(t_2-t_1-2\cdot\Delta t)\cdot e^{-\frac{C_1}{\tau+\epsilon_\tau}}} \tag{G.20}$$

Performing the same steps for (G.20) yields

$$\varepsilon_{mag} = \frac{A(t_1+\Delta t,t_2-\Delta t)\cdot\left(e^{-\frac{C_2}{\tau+\epsilon_\tau}}+1\right)-A(t_3-\Delta t,t_4+\Delta t)}{t_4-t_3+2\cdot\Delta t+(t_2-t_1-2\cdot\Delta t)\cdot(e^{-\frac{C_2}{\tau+\epsilon_\tau}}+1)} \tag{G.21}$$

Substituting the complete area expression described by

$$A(t_1+\Delta t,t_2-\Delta t) = \frac{-F_0\cdot\tau}{1-e^{-\frac{T}{\tau}}}\cdot(e^{-\frac{t_2-\Delta t}{\tau}}-e^{-\frac{t_1+\Delta t}{\tau}}) \tag{G.22}$$

in (G.20) and (G.21) yields respectively

$$\varepsilon_{mag} = \frac{-F_0\cdot\tau}{1-e^{-\frac{T}{\tau}}}\cdot\frac{(e^{-\frac{t_2-\Delta t}{\tau}}-e^{-\frac{t_1+\Delta t}{\tau}})\cdot e^{-\frac{C_1}{\tau+\epsilon_\tau}}-(e^{-\frac{t_4+\Delta t}{\tau}}-e^{-\frac{t_3-\Delta t}{\tau}})}{t_4-t_3+2\cdot\Delta t+(t_2-t_1-2\cdot\Delta t)\cdot e^{-\frac{C_1}{\tau+\epsilon_\tau}}} \tag{G.23}$$

and

$$\varepsilon_{mag} = \frac{-F_0\cdot\tau}{1-e^{-\frac{T}{\tau}}}\cdot\frac{(e^{-\frac{t_2-\Delta t}{\tau}}-e^{-\frac{t_1+\Delta t}{\tau}})\cdot\left(e^{-\frac{C_2}{\tau+\epsilon_\tau}}+1\right)-(e^{-\frac{t_4+\Delta t}{\tau}}-e^{-\frac{t_3-\Delta t}{\tau}})}{t_4-t_3+2\cdot\Delta t+(t_2-t_1-2\cdot\Delta t)\cdot(e^{-\frac{C_2}{\tau+\epsilon_\tau}}+1)} \tag{G.24}$$

G.2.3 Extraction of τ: measurement of two frequency-samples

Substituting $\varepsilon_1 = -\varepsilon_2 = \pm\varepsilon_{max}$ in (D.53), subtract τ and solve the result for ε_{max} yields the next derivation:

$$\epsilon_\tau = \sqrt{\frac{\left(\frac{|K|(\omega_2)-\varepsilon_{max}}{|K|(\omega_1)+\varepsilon_{max}}\right)^2 - 1}{\omega_1^2 - \left(\frac{|K|(\omega_2)-\varepsilon_{max}}{|K|(\omega_1)+\varepsilon_{max}}\right)^2 \cdot \omega_2^2}} - \tau \tag{G.25}$$

$$\rightarrow (\epsilon_\tau + \tau)^2 = \frac{\left(\frac{|K|(\omega_2)-\varepsilon_{max}}{|K|(\omega_1)+\varepsilon_{max}}\right)^2 - 1}{\omega_1^2 - \left(\frac{|K|(\omega_2)-\varepsilon_{max}}{|K|(\omega_1)+\varepsilon_{max}}\right)^2 \cdot \omega_2^2} \tag{G.26}$$

$$\left(\frac{|K|(\omega_2) - \varepsilon_{max}}{|K|(\omega_1) + \varepsilon_{max}}\right)^2 \cdot \left(1 + \omega_2^2 \cdot (\epsilon_\tau + \tau)^2\right) = \omega_1^2 \cdot (\epsilon_\tau + \tau)^2 + 1 \tag{G.27}$$

$$\left(\frac{|K|(\omega_2) - \varepsilon_{max}}{|K|(\omega_1) + \varepsilon_{max}}\right) = \sqrt{\frac{1 + \omega_1^2 \cdot (\epsilon_\tau + \tau)^2}{1 + \omega_2^2 \cdot (\epsilon_\tau + \tau)^2}} \tag{G.28}$$

$$\varepsilon_{max} \cdot \left(1 + \sqrt{\frac{1 + \omega_1^2 \cdot (\epsilon_\tau + \tau)^2}{1 + \omega_2^2 \cdot (\epsilon_\tau + \tau)^2}}\right) = |K|(\omega_2) - |K|(\omega_1) \cdot \sqrt{\frac{1 + \omega_1^2 \cdot (\epsilon_\tau + \tau)^2}{1 + \omega_2^2 \cdot (\epsilon_\tau + \tau)^2}} \tag{G.29}$$

$$\varepsilon_{max} = \frac{|K|(\omega_2) - |K|(\omega_1) \cdot \sqrt{\frac{1+\omega_1^2 \cdot (\epsilon_\tau+\tau)^2}{1+\omega_2^2 \cdot (\epsilon_\tau+\tau)^2}}}{1 + \sqrt{\frac{1+\omega_1^2 \cdot (\epsilon_\tau+\tau)^2}{1+\omega_2^2 \cdot (\epsilon_\tau+\tau)^2}}} \tag{G.30}$$

G.2.4 Extraction of τ: I and Q measurement

$$\frac{1}{2}(a_n + \varepsilon_{mag})\cos(\phi_{max}) + \frac{1}{2}(b_n - \varepsilon_{mag})\sin(\phi_{max}) = \frac{F_S F_0 \tau_\varepsilon}{1 + (n\omega_0\tau_\varepsilon)^2} \tag{G.31}$$

$$\frac{1}{2}(b_n - \varepsilon_{mag})\cos(-\phi_{max}) + \frac{1}{2}(a_n + \varepsilon_{mag})\sin(-\phi_{max}) = \frac{F_S F_0 \tau_\varepsilon^2 n\omega_0}{1 + (n\omega_0\tau_\varepsilon)^2} \tag{G.32}$$

Combining these expressions and solving this for ε_{mag} with $\tau_\varepsilon = \tau + \varepsilon_{tau}$ yields

$$\varepsilon_\tau = \frac{(b_n - \varepsilon_{mag})\cos(-\phi_{max}) + (a_n + \varepsilon_{mag})\sin(-\phi_{max})}{((a_n + \varepsilon_{mag})\cos(\phi_{max}) + (b_n - \varepsilon_{mag})\sin(\phi_{max}))\, n\omega_0} - \tau \tag{G.33}$$

$$\varepsilon_\tau = \frac{-\varepsilon_{mag}\left(\sin(\phi_{max}) + \cos(\phi_{max})\right) + b_n\cos(\phi_{max}) + a_n\sin(\phi_{max})}{\left(\varepsilon_{mag}\left(\cos(\phi_{max}) - \sin(\phi_{max})\right) + a_n\cos(\phi_{max}) + b_n\sin(\phi_{max})\right) n\omega_0} - \tau \tag{G.34}$$

Solving this for ε_{mag} yields

$$\begin{aligned}(\varepsilon_\tau + \tau)\cdot\left(\left(\varepsilon_{mag}\left(\cos(\phi_{max}) - \sin(\phi_{max})\right) + a_n\cos(\phi_{max}) + b_n\sin(\phi_{max})\right) n\omega_0\right) = \\ -\varepsilon_{mag}\left(\sin(\phi_{max}) + \cos(\phi_{max})\right) + b_n\cos(\phi_{max}) + a_n\sin(\phi_{max})\end{aligned} \tag{G.35}$$

$$\begin{aligned}\varepsilon_{mag}\left((\varepsilon_\tau + \tau)\cdot n\omega_0\left(\cos(\phi_{max}) - \sin(\phi_{max})\right) + \sin(\phi_{max}) + \cos(\phi_{max})\right) = \\ -(\varepsilon_\tau + \tau)\cdot n\omega_0\left(a_n\cos(\phi_{max}) + b_n\sin(\phi_{max})\right) + b_n\cos(\phi_{max}) - a_n\sin(\phi_{max})\end{aligned} \tag{G.36}$$

$$\varepsilon_{mag} = \frac{-(\varepsilon_\tau + \tau)\cdot n\omega_0\left(a_n\cos(\phi_{max}) + b_n\sin(\phi_{max})\right) + b_n\cos(\phi_{max}) - a_n\sin(\phi_{max})}{(\varepsilon_\tau + \tau)\cdot n\omega_0\left(\cos(\phi_{max}) - \sin(\phi_{max})\right) + \sin(\phi_{max}) + \cos(\phi_{max})} \tag{G.37}$$

Substituting (D.36) and (D.37) for respectively a_n and b_n in (G.37) yields

$$\varepsilon_{mag} = \frac{-(\varepsilon_\tau + \tau)\cdot n\omega_0\left(\cos(\phi_{max}) + \tau n\omega_0\sin(\phi_{max})\right) + \tau n\omega_0\cos(\phi_{max}) - \sin(\phi_{max})}{(\varepsilon_\tau + \tau)\cdot n\omega_0\left(\cos(\phi_{max}) - \sin(\phi_{max})\right) + \sin(\phi_{max}) + \cos(\phi_{max})} \cdot \frac{2F_S F_0 \tau}{1 + (n\omega_0\tau)^2} \tag{G.38}$$

Bibliography

[1] Periasamy A. and Clegg R.M. *FLIM Microscopy in Biology and Medicine*, volume 1st. CRC Press, 07 2009. ISBN 9781420078909.

[2] Korterik J. Labview real-time simulation. 3 2010.

[3] van Munster, E.B. and Gadella, T.W.J. Fluorescence lifetime imaging microscopy (flim). *Adv Biochem Engin/Biotechnol*, pages 143–175, 2005.

[4] Pelgrom J.M. *Analog-toDigital Conversion*, volume 1st. Springer, 07 2010. ISBN 9048188873.

[5] B. Razavi. *RF microelectronics*, volume 1. Prentice Hall PTR, 12 1998. ISBN 0-13-887571-5.

[6] B. Razavi. *Design of Integrated Circuits for Optical Communications*, volume 1. The McGraw-Hill Companies, 12 2003. ISBN 0-07-282258-9.

[7] T. Sepke, P. Holloway, C.G. Sodini, and H.-S. Lee. Noise analysis for comparator-based circuits. *Circuits and Systems I: Regular Papers, IEEE Transactions on*, 56(3):541 –553, 2009. ISSN 1549-8328. doi: 10.1109/TCSI.2008.2002547.

[8] J.R. Lakowicz. *Principles of fluorescence spectroscopy*. Springer, 2006. ISBN 978-0-387-31278-1.

[9] Martin Straume, Susan Frasier-Cadoret, and Michael Johnson. Least-squares analysis of fluorescence data. In Chris D. Geddes, Joseph R. Lakowicz, and Joseph Lakowicz, editors, *Topics in Fluorescence Spectroscopy*, volume 2 of *Topics in Fluorescence Spectroscopy*, pages 177–240. Springer US, 2002. ISBN 978-0-306-47058-5.

[10] R.J. Beerends, H.G. ter Morsche, J.C. van den Berg, and E.M. van de Vrie. *Fourier and Laplace Transforms*, volume 1st. Cambridge University Press, 07 2003. ISBN 0521534410.

[11] Xiang Gao, E.A.M. Klumperink, P.F.J. Geraedts, and B. Nauta. Jitter analysis and a benchmarking figure-of-merit for phase-locked loops. *Circuits and Systems II: Express Briefs, IEEE Transactions on*, 56(2):117 –121, 2009. ISSN 1549-7747. doi: 10.1109/TCSII.2008.2010189.

[12] MAXIM. *Converting between RMS and Peak-to-Peak Jitter at a Specified BER*. MAXIM, 07 2000.

[13] S. Gupta, M. Choi, M. Inerfield, and Jingbo Wang. A 1gs/s 11b time-interleaved adc in 0.13/spl mu/m cmos. In *Solid-State Circuits Conference, 2006. ISSCC 2006. Digest of Technical Papers. IEEE International*, pages 2360 –2369, 2006. doi: 10.1109/ISSCC.2006.1696299.

[14] N. Da Dalt, E. Thaller, P. Gregorius, and L. Gazsi. A low jitter triple-band digital lc pll in 130nm cmos. In *Solid-State Circuits Conference, 2004. ESSCIRC 2004. Proceeding of the 30th European*, pages 371 – 374, 21-23 2004. doi: 10.1109/ESSCIR.2004.1356695.

[15] Kuo-Hsing Cheng, Yu-Chang Tsai, Kai-Wei Hong, and Yen-Hsueh Wu. A low jitter self-calibration pll for 10gbps soc transmission links application. In *Electronics, Circuits and Systems, 2008. ICECS 2008. 15th IEEE International Conference on*, pages 786 –789, aug. 2008. doi: 10.1109/ICECS.2008.4674971.

[16] Manxia Xiao, Ning Li, Fan Ye, and Junyan Ren. A 1.2v low-jitter pll for uwb. In *ASIC, 2007. ASICON '07. 7th International Conference on*, pages 323 –326, 22-25 2007. doi: 10.1109/ICASIC.2007.4415632.

[17] J. Stewart. *Calculus-early*, volume 5th. Cambridge University Press, 12 2002. ISBN 053439339X.